60-years drought analysis of meteorological data in the western Po river Basin

Emanuele Mombrini[1], Stefania Tamea[1], Alberto Viglione[1], and Roberto Revelli[1,†]

[1]Dipartimento di Ingegneria dell'Ambiente, del Territorio e delle Infrastrutture (DIATI), Politecnico di Torino, Torino.
[†]deceased, 6 May 2023

Correspondence: Emanuele Mombrini (emanuele.mombrini@polito.it)

Abstract. Since the start of the 21st century, increasing focus has been put on drought and its wide range of environmental and socioeconomic effects, particularly in the context of climate change. This is especially true for the North-western region of Italy, comprising the Piedmont and Aosta valley, which have been affected in recent years by droughts that have had acute effects on water resources and water security in all sectors, including agriculture, energy and domestic use. The region also belongs to the Mediterranean climate hot-spot, characterized by faster than global average warming rates and higher vulnerability to their effects. Therefore, characterizing the observed changes and trends in drought conditions is of particular significance. To this end, 60 years of precipitation and temperature data are first analyzed to identify trends, finding limited areas with significant precipitation decrease and, conversely, a general temperature increase over the region, with higher values found in the higher elevation areas. The drought indices SPI (Standardized Precipitation Index) and SPEI (Standardized Precipitation Evapotranspiration Index) at a short (3-month) and long (12-month) time scale are then calculated and analyzed. Changes in meteorological drought are evaluated, both in terms of drought indices trends and in terms of changes in the characteristics of drought periods, on both a local and regional scale. Relations between terrain characteristics of the area and the observed changes are highlighted, with significant differences between the plain and mountainous portion of the region. The differences are mainly related to the observed trends, with the flat low-altitude part of the region displaying a tendency towards dryer conditions, not shared with the mountainous area. Significantly, no trend is found at a region-wide level but is instead found when considering homogeneous areas defined by terrain characteristics. Furthermore, changes in the number of drought episodes and in their severity, duration and intensity are found to be correlated with terrain characteristics at all time scales.

1 Introduction

Drought is considered to be one of the main natural disasters, with widespread effects affecting large portions of the world's population (Wallemacq et al., 2015) and causing severe financial losses (García-León et al., 2021) and ecosystem impacts (Crausbay et al., 2020). Drought also has both short- and long-term effects on water availability (IDMP, 2022), which are relevant when considering the global increase in water demand in the last 100 years and the predicted challenges in meeting that demand in the future (Unesco, 2018; Wada et al., 2016; Burek et al., 2016).

These drought-related phenomena are also likely to become more intense, as droughts are predicted to become more severe and frequent under climate change conditions (Dai, 2011, 2013; Trenberth et al., 2014; Ward et al., 2020; Pörtner et al., 2022). Understanding how and where changes will occur on a local scale is thus necessary in order to develop adequate adaptation responses. Several studies on meteorological drought trends in the northern Italian peninsula—often in the context of the wider Mediterranean or alpine region—have been carried out, analyzing either precipitation series (Bordi and Sutera, 2002; Brunetti et al., 2002; Hoerling et al., 2012; Haslinger and Blöschl, 2017; Pavan et al., 2019) or precipitation and temperature series (Hanel et al., 2018; Falzoi et al., 2019; Arpa Piemonte and Regione Piemonte, 2020b; Baronetti et al., 2020; Vogel et al., 2021). Overall, these studies have found an increase in meteorological drought occurrence in North-West Italy, particularly after the 1970s, even when recent drought events have not been found to be exceptional when compared to historical records (Haslinger and Blöschl, 2017; Hanel et al., 2018). Regarding the underlying changes in precipitation, their reported seasonality differs significantly, with precipitation decrease found either in the winter (Brunetti et al., 2002; Hoerling et al., 2012)or summer season (Haslinger et al., 2012; Hanel et al., 2018; Pavan et al., 2019). On the other hand, studies considering temperature values have consistently shown rising temperatures, and thus a rise in evaporative demand, to be a main factor in drought increase, even when significant changes in precipitation patterns were detected.

In addition to this focus on drought trends in wider areas, interest in regional expressions of climate change has been growing. One of the most investigated of these regional phenomena is the enhancement of warming rates with elevation, known as elevation dependent warming, on which many studies have been performed in recent decades: for a summary of studies based on surface measurement, see Mountain Research Initiative EDW Working Group (2015); for a summary of studies based on climate models, see Palazzi et al. (2019). In general, despite conflicting results regarding the presence of an elevation effect on warming rates and the lack of adequate climate data for mountainous regions, a consensus on enhanced warming rates at higher altitudes emerges (Rangwala and Miller, 2012; Pepin et al., 2022). Orographic precipitation gradients, i.e. the elevation-dependency of precipitation change, while less understood, have also been widely investigated, with less consensus on the results. A comprehensive meta-analysis of both in-situ studies of precipitation data from mountainous regions (including the Alps) and of global gridded databases from the early 1950s to the late 2010s reported a relative decrease in precipitation compared to lowlands, although without high confidence (Pepin et al., 2022). Furthermore, analyses such as Giorgi et al. (2016) have shown the importance of spatial resolution in understanding these processes in topographically complex regions, reporting that increases in summer precipitation in higher elevation areas of the Alpine range could only be detected by high resolution regional climate models and observed by high resolution observation networks.

Understanding the possible effects of topographically related phenomena on drought conditions is thus of particular interest in an area such as the western Po river basin, which comprises both wide plains and high mountains. Despite the presence, as detailed above, of studies on drought in the chosen region, these lacked either the needed spatial resolution or focus to evaluate possible effects of terrain characteristics on drought conditions. In this study, possible correlations between topographical characteristics—both mean elevation and terrain ruggedness—and drought are evaluated, both in terms of the distribution of wetting/drying trends, and in terms of different dynamics (duration, severity, intensity) of drought periods. Results obtained by

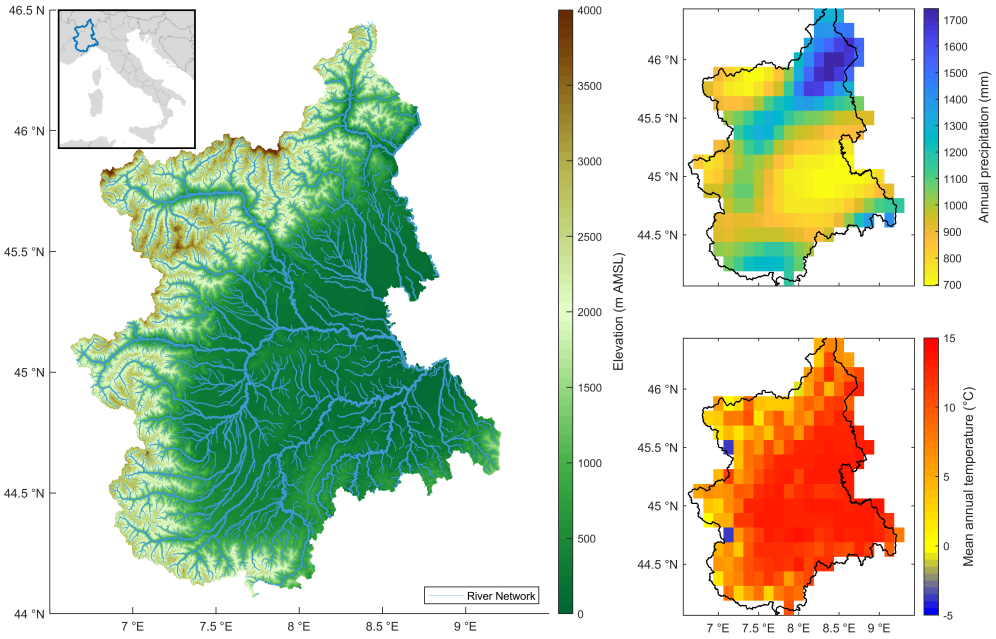

Figure 1. Map of the study area, including elevation, river network, mean annual precipitation and mean temperature values.

focusing on either mean elevation or terrain ruggedness are also compared, to understand if only elevation-related effect are present, or rather more complex interactions between meteorological drought and terrain characteristics. To this end, a grid data set of precipitation and temperature values obtained from a dense network of gauging stations distributed at different elevations throughout the domain and spanning more than 60 years is analyzed by calculating the SPI and SPEI at a shorter 3 month time scale and at a longer 12 month time scale. The index series are analyzed in order to find trends in drought conditions, as well as changes in drought characteristics both on a local and on a region-wide level.

In Section 2 the study area, as well as the analyzed data set are presented; the analysis methods used are also discussed, including the derived SPI and SPEI indices. In Section 3 the results obtained from each analysis are reported, while in Section 4 the general conclusion derived from the study are discussed.

2 Materials and methods

2.1 Study area

The Piedmont region and the Aosta valley (Figure 1) are situated in the north-west of Italy, bordered by France on the west and south-west, Switzerland on the north, and two other Italian regions (namely Lombardia and Liguria) on the east and south-east. Although divided in two administrative regions, they together represent the head of the Po river basin, as well as the Italian north-western side of the alpine chain; furthermore, the main valley in the Aosta region leads directly into the Piedmont

territory. Therefore they are going to be treated as one domain for this study. The Piedmont part of the domain covers more than 25000 km^2, while The Aosta Valley part covers 3200 km^2. Orographically, it is mainly a mountainous region, surrounded by the Alpine chain from the south-east, throughout the western front, up to the norther point. Mountainous reliefs occupy half of its territory, with the highest peaks lying in the Aosta Valley, while the Po plain lies in the central and eastern part of the region. Due to the small latitude variation throughout the area, the area's reliefs plays a key role in defining the area's climate variability (Arpa Piemonte, 2007): continental air masses from the Po plain, moist currents from the Mediterranean sea and north-western Atlantic currents interact with the reliefs leading to a complex and spatially variable climate (Ciccarelli et al., 2008). Precipitation is characterized by a bimodal distribution, with maxima in spring and autumn, and minima in summer and winter. For most of the region (close to 90%) winter is the season with the absolute minimum precipitation, and only for the south west corner the absolute minimum is in summer; for the western and southern side of the territory (close to 60% of the overall area) the highest precipitations occur in autumn, while for the central-eastern part they occur in spring (Perosino and Zaccara, 2006). Annual precipitation ranges from 700 to more than 1700 mm, with a mean of 1000 mm. Annual precipitation is lowest in the central-west area and in the Aosta Valley, while highest in the norther area (Figure 1). Mean annual temperatures range from slightly over 13°C near the eastern border to slightly under -3.6°C, closely following the altitude of the area; the diurnal temperature range varies from 2 °C to more than 12 °C, is highest in summer, and is also generally inversely correlated with elevation.

2.2 Data source and data processing

The data used in the analysis is obtained from the North Western Italy Optimal Interpolation (NWIOI) data set (Arpa Piemonte, Dipartimento Sistemi Provisionali, 2011), calculated and published by the Forecast Systems Department of the Regional Environmental Protection Agency of Piedmont (*Dipartimento Sistemi Previsionali - Arpa Piemonte*). The data set contains daily precipitation, maximum and minimum temperature values over a regular grid covering the domain area with a 0.125° resolution. The data is obtained through an analysis of the region's meteorological station network data via the Optimal Interpolation method (Uboldi et al., 2008). The method spatially interpolates station data by correcting a previously defined background field based on an "area of influence" for each station. This area of influence is both horizontal and vertical in the case of temperature stations (tri-dimensional interpolation) and only horizontal in the case of precipitation stations (two-dimensional interpolation). In any case, no direct trend relation between the meteorological values and elevation has been evaluated and removed/added from the data (further details on the Optimal Interpolation method and its calibration are given in Appendix A). The data used in the interpolation method is provided by a dense gauging network (roughly 200 stations) covering both low and high altitude areas, providing a much higher number of stations than other available datasets for the area (Turco et al., 2013).

For the purpose of the subsequent analysis, 227 (the number of grid points inside the domain) series of 783 monthly values (December 1957 - February 2023) of precipitation, maximum and minimum temperature are calculated.

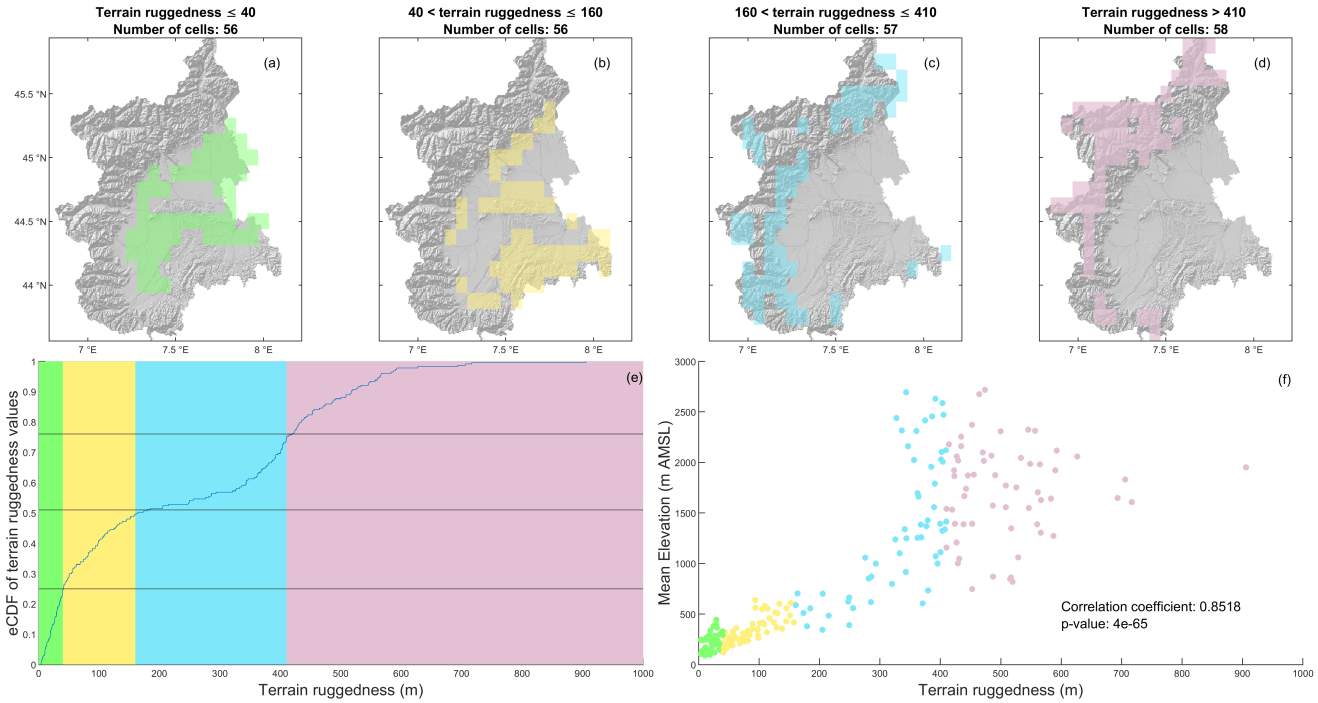

Figure 2. Areas classified using terrain ruggedness, calculated as the standard deviation of elevation values inside each cell. **(a-d)** Areas belonging to classes defined based on terrain ruggedness, corresponding to the A to D areas cited in the following figures. **(e)** Empirical cumulative distribution function (eCDF) of the terrain ruggedness values. **(F)** Scatter plot between terrain ruggedness and mean elevation for each cell and relative Pearson correlation coefficient.

2.3 Area definition based on elevation

In order to study possible correlations between meteorological characteristics (trends in precipitation, temperature and drought indices) and terrain characteristics, elevation values for the studied domain are obtained using the EarthEnv-DEM90 digital elevation model (Robinson et al., 2014) with 90 m resolution. Two sets of values are then obtained for each grid cell: the mean elevation (average of the elevation values inside a cell) and the terrain ruggedness. The terrain ruggedness (also known as surface roughness or topographic hetereogenity) is defined as the "deviations in the direction of the normal vector of a real surface from its ideal or intended form" (Whitehouse, 1994), meaning the irregularity of a landscape; similarly to other studies, it is here calculated as the standard deviation of the elevation values inside every grid cell (Habib, 2021). Both mean elevation and terrain ruggedness values are also used to define four distinct areas of an almost equal number of cells (Figure 2); in the case of the terrain ruggedness values, these represent the plains, the hilly region, and the lower and higher mountains respectively. Significantly, this latter classification was able to distinguish the hills in the center-south of the region from the eastern flat part of the region, despite similar mean elevation. Regardless of its simplicity, the classification, when considering

the precipitation and temperature grid resolution, is quite satisfactory for the purposes of this study, and it is consistent with the K3 Mountain classification (Karagulle et al., 2017), a much more complex categorization based on many different parameters, obtained from Global Mountain Explorer 2.0 platform (Sayre et al., 2018).

2.4 Data analysis techniques

2.4.1 Standardized Precipitation Index (SPI)

Monthly precipitation values are used to calculate the Standardized Precipitation Index (McKee et al., 1993) at 3 and 12 month scale. The probability distribution chosen for the index calculation is the gamma distribution because, although other possible distributions have been proposed in the literature (Angelidis et al., 2012), including empirical ones (Laimighofer and Laaha, 2022), no single one was shown to be markedly better than the gamma distribution. Following the standard procedure found in the literature (Tigkas et al., 2015; Angelidis et al., 2012; Bordi and Sutera, 2002; Hayes et al., 1999), the index is thus obtained by fitting the gamma probability distribution $f(x) = \frac{1}{\Gamma(a)b^a} x^{a-1} e^{-x/b}$ to each month-of-the-year's series of values. To do this, the shape parameter a and the scale parameter b of the gamma distribution are calculated for each series of non-zero values of each month using the maximum likelihood method (Choi and Wette, 1969). The cumulative probability F_X is calculated as:

$$F_X(x_{i,j}) = \int_0^{x_{i,j}} f(x_{i,j})\,dx = \frac{1}{b_j^{a_j}\Gamma(a_j)} \int_0^{x_{i,j}} x_{i,j}^{a_j-1} e^{-x_{i,j}/b_j}\,dx \tag{1}$$

where j is the month index ($j = 1, 2...12$), i is the year index ($i = 1, 2...n$, with n years of records), and $\Gamma(a_j)$ is the gamma function, i.e. $\int_0^\infty y^{a_j-1} e^{-y}\,dy$.

To take the probability of zero values into account (given that the gamma distribution is defined for $x \in (0, \infty)$), the zero-inflated model is defined as:

$$H_X(x_{i,j}) = q_j + (1 - q_j) F_X(x_{i,j}) \tag{2}$$

where q_j is the probability of zero precipitation for the j-th month of the year. Finally, the SPI is calculated as the normal inverse function of H_X via the formula:

$$SPI(x_{i,j}) = -\sqrt{2}\Phi^{-1}(H_X(x_{i,j})) \tag{3}$$

where $\Phi^{-1}v$ is the inverse of the complementary error function:

$$\Phi(x) = \frac{2}{\sqrt{\pi}} \int_x^\infty e^{-t^2}\,dt \tag{4}$$

The SPI obtained through this method is thus a series of positive and negative values belonging to a normal distribution ($\mu = 0$, $\sigma = 1$): negative (positive) values represent precipitation below (above) the mean, with values lower than -1 denoting drought conditions (World Meteorological Organization, 2012). To calculate the index at a different time scale, a moving average is

first applied to the each monthly value, with length equal to the desired time scale and only previous data included; data that doesn't have enough preceding values to calculate the moving average is discarded. After calculating SPI on this data, each monthly value of the index describes how the conditions for a period with length equal to the time scale and ending in one particular month compares with all others in the series. For example, the SPI at 3 month time scale (SPI-3) for the month of July of a particular year indicates how much dry/wet the the previous 3 months have been compared with all other May-July periods in the series.

Finally, in-built Matlab® functions are used for both the incomplete gamma function and its scale and shape parameters calculation and the calculation of the normal inverse function.

2.4.2 Standardized Precipitation Evapotranspiration Index (SPEI)

In order to take into account the effect of evaporative demand on drought episodes, and for comparison with SPI values, the Standardized Precipitation Evapotranspiration Index (Vicente-Serrano et al., 2010) is calculated at 3 and 12 month scale. The procedure for calculating the index is the same as the SPI, but the data analyzed is a series of monthly precipitation minus reference evapotranspiration (ET_0, in mm) values and a log-logistic probability distribution is used. Temperature data was used to calculate monthly ET_0 values using the Hargreaves formula (Hargreaves and Samani, 1985), following the recommendations for SPEI calculation (Beguería et al., 2014). Probability Weighted Moments (PWMs) using Hosking's unbiased method (Hosking, 1986) were used to calculate the α, β and γ parameters of the log-normal distribution for each month of the year, according to the formulae (again according to the recommendations for the index calculations found in Beguería et al., 2014):

$$w_{s_j} = \frac{1}{N}\sum_{i=1}^{N}\frac{\binom{N-i}{s}d_{i,j}}{\binom{N-1}{s}} \tag{5}$$

$$\beta_j = \frac{2w_{1_j} - w_{0_j}}{6w_{1_j} - w_{0_j} - 6w_{2_j}} \tag{6}$$

$$\alpha_j = \frac{(w_{0_j} - 2w_{1_j})\beta_j}{\Gamma(1+1/\beta_j)\Gamma(1-1/\beta_j)} \tag{7}$$

$$\gamma_j = w_{0_j} - \alpha_j\Gamma(1+1/\beta_j)\Gamma(1-1/\beta_j) \tag{8}$$

where $d_{i,j}$ are the precipitation minus ET_0 values for a given month j of the year i and w_{s_j} are the s order of the PWM for the month j. Using the α_j, β_j and γ_j parameters the log-logistic distribution is calculated as:

$$F_D(d_{i,j}) = \left[1 + \left(\frac{\alpha_j}{d_{i,j} - \gamma_j}\right)^{\beta_j}\right]^{-1} \tag{9}$$

Finally, this F_D distribution is then transformed into a normal distribution to obtain the SPEI values. Again, moving average windows are applied to the input data in order to obtain different time scales. The distribution was shown to be well suited to analyze the data, as calculations obtained a finite solution for all series.

2.4.3 Trend analysis

Drought index series, annual and seasonal precipitation series, as well as deseasonalized and seasonal maximum and minimum temperature series, are analyzed in order to search for significant (at 5% significance) trends. Seasonal values are defined as the cumulative precipitation values and the mean temperature values over the four three-months periods December-January-February (Winter), March-April-May (Spring), June-July-August (Summer), September-October-November (Fall). Furthermore, deseasonalization is performed by subtracting the mean of the detrended temperature series for each month using the Climate Data Toolbox (Greene et al., 2019). In all cases, but particularly for drought indices, the autocorrelation of the series (given that a moving average is applied at 3 and 12 month time scale) is taken into account by also applying different pre-whitening methods before performing trend analysis. These method are the simple Pre-Whitening method (PW, Kulkarni and Storch, 1995), the Trend Free Pre-Whitening method (TFPW, Yue et al., 2002) and the Variance Corrected Trend Free Pre-Whitening method (VCTFPW, Wang et al., 2015). The different results are used to obtain one trend evaluation by applying the 3PW algorithm (Collaud Coen et al., 2020), which, for the purpose of this study, is as follows:

1. If the lag-1 autocorrelation of the data is significant (following a normal distribution at the two-sided 95 % confidence interval), the PW and TFPW series are obtained from the original series.

2. The trend is considered significant if both processed series return significant trends; the significance is chosen as the lower of the PW and TFPW series calculated via the Mann-Kendall test.

3. The slope of the significant trend is given as the Sen's slope of the VCTFPW series.

If the lag-1 autocorrelation of a series is found not to be significant, trend analysis is performed on the un-modified data.

2.4.4 Local drought analysis

Each SPI/SPEI series, at both time scales, is analyzed through a *run analysis* in order to study local drought characteristics. Based on run theory (Yevjevich, 1967), run analysis defines a drought run as a series of consecutive months under a certain threshold (-1, corresponding to a moderately dry condition in the SPI classification). Adding onto this definition, the negative values leading and following a period under the -1 threshold are counted as part of the runs, in order to capture events where a deficit is not fully recovered from. The differences between the use of a single threshold and the inclusion of the run onset and offset are shown in Figure 3: the method used in the present study considers two periods of months with index value under the -1 threshold as part of the same run if the drought index remains lower than 0 between them; in any case, a drought run ends if the drought index becomes positive. Drought run characteristics are then calculated for each local drought (Caloiero et al., 2021):

- Drought Duration (DD_L) is the length of the drought run, reported in months for this study;

- Drought Severity (DS_L) is the cumulative value of the index during each run;

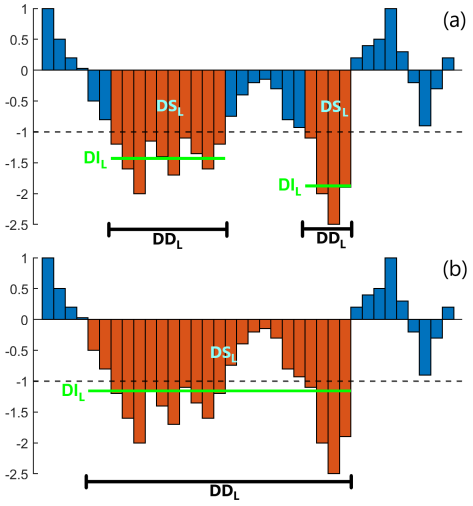

Figure 3. Drought runs examples, highlighted in orange. **(a)** Runs obtained with a simple -1 threshold (not used in this paper). **(b)** Run defined by a threshold and by including including their onset and offset, i.e. all negative values before and after the values under the threshold (as used in this paper). In both cases DS_L is the sum of the index value during the run, DD_L is the length of each run and DI_L is the mean index value during the run.

– Drough Intensity(DI_L) the ratio between the DS_L and DD_L value of a run, i.e. the average index value during the run.

Given a series of drought runs calculated from an index series, the average value of these characteristics for all runs are reported as $\overline{DD}_L$, $\overline{DS}_L$ and $\overline{DI}_L$. Pedex L indicates that these are *local* drought characteristics, as opposed to drought characteristics calculated over multiple grid points.

2.4.5 Region-wide drought event analysis

In order to study the spatio-temporal characteristics of drought, and to define region-wide drought events, drought indices are analyzed in a similar way to that proposed in González-Hidalgo et al. (2018), Baronetti et al. (2020) and Baronetti et al. (2022). To contrast with local droughts, which are calculated from a series of index values belonging to one cell, droughts evaluated through this method are called *region-wide drought events*. So, for example, during a region-wide drought event a certain percentage of the domain will be in drought conditions (below the -1 drought index threshold); each of these cells will therefore be experiencing a local drought. Region-wide drought events are detected through the use of two thresholds (the minimum duration threshold of 3 weeks, used in the cited papers, is always met as monthly data is used in this analysis):

– an index threshold, based on the SPI/SPEI values: cells with an index lower than -1 are considered to be in drought condition;

– an area threshold: a drought episode is considered in progress when at least 25% of the domain is in drought condition.

In addition to these two thresholds, the drought events' *onset* and *offset*, meaning the periods below the 25% drought area threshold before and after a period above the threshold, were also included in the the drought event itself. This approach is useful in considering persisting drought conditions as one continuous event while still maintaining well-defined episodes, similar to the proposed local drought definition (see Figure 3).

Similarly to local drought, different characteristics are calculated for each region-wide drought event:

- Drought event Duration (DD_E) is the length of the drought event;
- Drought event Severity (DS_E) is the sum of the drought index of each cell in drought condition for the duration of the event, divided by the total number of cells in the domain;
- Drought event Intensity (DI_E) is the mean of the local intensity for each cell that has been part of the drought event. Intensity for each cell is calculated as the sum of the drought index below the -1 threshold divided by the number of months where the index was lower than -1.
- Drought Area (DA_E) is the average number of cells in drought condition during the event;

Given a series of region-wide drought events calculated from the index series for all cells in the domain, the average value of these characteristics for all events are reported as $\overline{DD}_E$, $\overline{DS}_E$, $\overline{DI}_E$ and $\overline{DA}_E$.

2.4.6 Correlation analysis

Possible correlation between terrain characteristics and trend values as well as drought characteristics are studied by calculating both the Pearson and the Spearman correlation coefficients (Shevlyakov and Oja, 2016). In all cases where correlation values are reported, scatter plots of the two variables are checked (even if not shown here) to check deviations from linearity of correlation. Given that the correlation values obtained with the two methods do not differ strongly, with Spearman correlation values generally being higher, only Pearson's correlation values are reported in the following paragraphs.

2.4.7 Change analysis of drought characteristics

In order to evaluate the significance of the change in average drought characteristics between the periods 1958-1990 and 1990-2023 (approximately the first and second half of the series), the two sample t-test (Rasch et al., 2011) is applied to $\overline{DS}_L$, $\overline{DD}_L$ and $\overline{DI}_L$ (as well as $\overline{DS}_E$, $\overline{DD}_E$, $\overline{DI}_E$ and $\overline{DA}_E$) calculated for the drought periods starting before and after January 1990, respectively. After obtaining the values pre and post 1990, their sample mean and standard deviations are calculated, and the test statistic t is calculated as

$$t = \frac{\overline{DC}_{post} - \overline{DC}_{pre}}{s} \tag{10}$$

where $\overline{DC}$ is the mean of a certain drought characteristics for all drought runs/events before/after 1990 and s:

$$s = \sqrt{\frac{\sigma^2_{post}}{n_{post}} + \frac{\sigma^2_{pre}}{n_{pre}}} \tag{11}$$

where σ is the standard deviation of a certain drought characteristics for all drought run/events before and after 1990 and n the number of run/events for the two periods. t is then compared with the critical value of the statistic at a 5% significance level. Given that no assumptions about the variance of the two ensembles were made, and given the different number of runs in the two periods, the degrees of freedom needed for the calculation of the critical value were approximated through the Welch-Satterthwaite equation (Welch, 1947).

3 Results

3.1 Precipitation and temperature trends

The precipitation and temperature data used to calculate the SPI/SPEI is first analyzed in order to find possible trends, to contextualize the results obtained from the drought indices. For the most part, changes in both annual (Figure 4a-b) and seasonal (supplementary material B1) precipitation values for the Piedmont and Aosta Valley region are found not to be statistically significant; furthermore, no significant difference is found between absolute trends in mm/year and trends relative to the 1958-1990 mean. Only some portions of the region, bordering on the Alpine chain in the north and south, show significant trends, mostly reporting reduced precipitation. The main difference is found in the winter season (Figure B1a), where 30% of cells, covering a large part of the southern half of the region, report decreases as high as -2.41 mm/year, but mostly around -1.2 mm/year (-0.86% and -0.47% in relative terms to the 1958-1990 mean respectively). Conversely, a small region in the north-east of the domain reports negative precipitation trends in the spring and summer seasons (mean decrease of -2.12 and -1.81 mm/year ,- 0.62 % and -0.67 % in relative term to the 1958-1990 mean, for spring and summer respectively) but not in winter (supplementary Figure B1b-c). Still, spatially averaged precipitation over the whole region does not show a statistically significant decrease either at the annual or seasonal scale.

In contrast to precipitation values, all of the region is found to be affected by significant temperature trends (Figure 4c-d). Maximum temperature is rising all over the domain, from 0.008 to 0.065 °C/year, with a mean of 0.03 °C/year; this rate of increase is significantly correlated with mean elevation (0.38 correlation value with p-value equal to 1.96×10^{-7}), although a small zone, in the flat part of the region on the western border, shows slope coefficients comparable with those with a higher mean elevation.

Minimum temperatures, while overall still increasing, present less homogeneous results. First, 6.6% of cells, mainly grouped at the center of the region, show a negative trend; furthermore 16% of cells show no significant trend. Minimum temperature change ranges from -0.02 to 0.07 °C/year, with a mean of 0.02 °C/year, and also shows a significant correlation with mean elevation, although with a lower 0.16 correlation value and a 0.04 p-value. Seasonal analysis largely reflects the results for both minimum and maximum annual temperature, while showing the highest seasonal increases in winter (shown in supplementary Figure B2 and B3). Coherently with local results, maximum and minimum temperatures for the whole region are found to be increasing at a rate of 0.03 and 0.02 °C/year, respectively.

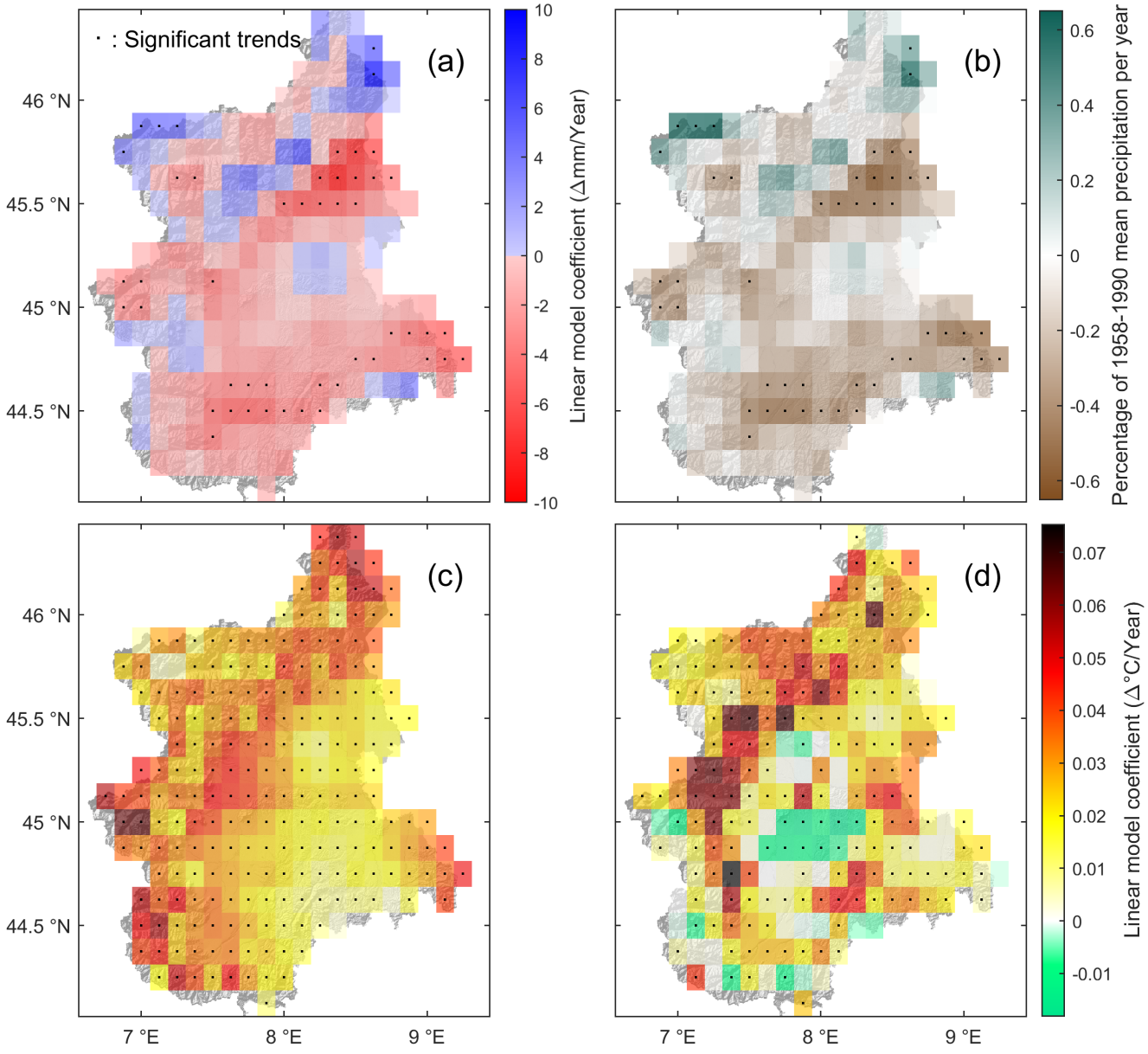

Figure 4. Results of trend analysis on meteorological data for the Piedmont and Aosta valley region. **(a)** Annual precipitation trends in absolute terms, **(b)** annual precipitation trends in units of relative change compared to the 1958–1990 mean precipitation, **(c)** maximum monthly temperature trends, **(d)** minimum monthly temperature trends. Cells containing a dot denote significant trends at 5% significance.

The reported results, both for the precipitation and temperature trends, are in agreement with the analysis made on the same data set by the local environmental agency (*Arpa Piemonte*, 2020a) and with the results obtained from studies conducted on the Piedmont and Aosta Valley meteorological station network data (Ciccarelli et al., 2008; Acquaotta et al., 2009), and particularly on high elevation stations' data (Acquaotta et al., 2015; Terzago et al., 2013).

3.2 Drought indices trends

Drought indices calculated from the precipitation and temperature series of each cell in the region are analyzed in order to find possible trends in drought conditions. Given the nature of SPI, as described in Section 2.4.1, negative trends indicate a tendency for precipitation to be below the series's mean value. This means that both wet and dry periods have seen on average reduced precipitation, and thus that droughts conditions, when occurring, have become worse. For the SPEI, described in Section 2.4.2, the trend interpretation is the same, but instead of precipitation a climatic water balance between precipitation and potential evapotranspiration is considered. Furthermore, trend analysis on indices at the shorter 3 month time scale and the longer 12 months time scale indicates, respectively, how drought conditions might have evolved over smaller time scales, closer to the response time of soil moisture conditions to meteorological conditions, and over larger time scales, closer to the response time of water reservoirs and groundwater levels to meteorological conditions.

Trend analysis on SPI-3 and SPI-12 values shows results that mostly agree with the trends in annual precipitation, as a majority of cells reports both significant negative trends in annual precipitation values and in index values (and thus a tendency towards dryer conditions). A majority of cells (almost 70%) shows negative SPI trends at both 3 and 12 months time scale, although SPI-12 indicates dryer conditions over time compared to SPI-3 (Figure 5a-b).

Trend analysis for SPEI-3 and SPEI-12 displays a similar time scale effect, with the longer time scale having a higher number of cells with significant trends (although with 79% of cells showing trends for both time scales) and, on average, greater slope coefficients (Figure 5c-d).

The clearest differences emerge by comparing the results obtained by SPI and SPEI (Figure 5e). The latter shows, at both time scales, a far wider region heading towards dryer conditions (more than twice the cells found with SPI), and at a faster rate, given the slope coefficients. Furthermore, a clear relation between terrain characteristics and trends becomes apparent from the SPEI analysis, that shows, contrary to the mountainous areas, most of the flat part of the region is affected by significant trends (Figure 5f).

The importance of terrain characteristics in determining the significance of trends is also evaluated by performing a trend analysis separating four different areas according to terrain ruggedness, namely the flat, hilly, and mountainous areas (as defined in Section 2.3). The drought indices, calculated from cumulative precipitation and mean temperature for the four areas, show a clear difference in observed trends. The flat part of the region reports significant drying trends for both SPI-12, SPEI-3 and SPEI-12, despite the trend in annual precipitation being not significant and the temperature trends having a lower slope coefficient than at higher altitudes (Figure 6). Conversely, the alpine chain reports no significant trends in the indices,

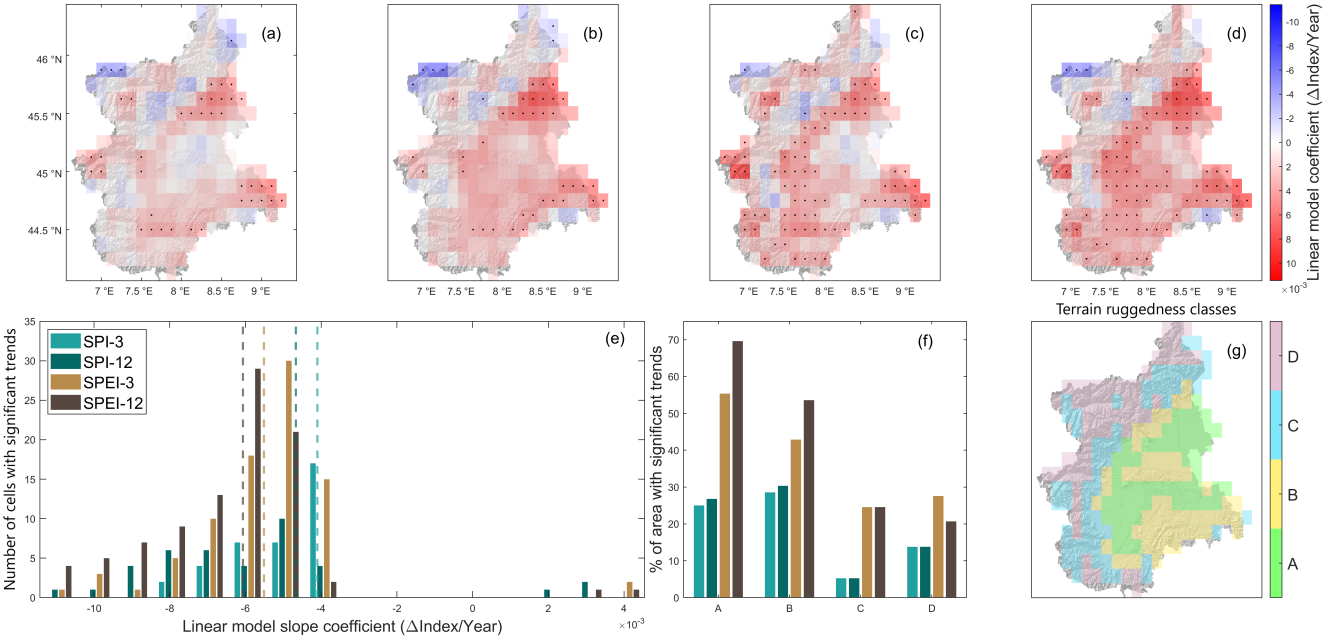

Figure 5. Trend analysis on drought indices. **(a)** SPI-3 trends. **(b)** SPEI-3 trends. **(c)** SPI-12 trends. **(d)** SPEI-12 trends. Cells containing a dot denote significant trends at 5% significance. **(e)** Frequency histogram of significant trends per distribution of trends' Sen-slope coefficients, with dashed lines representing the respective mean values of indexes. **(f)** Frequency histogram per class of terrain ruggedness (for cells with significant trends). **(g)** Representation of terrain ruggedness classes (see Figure 2 for more details on their definition).

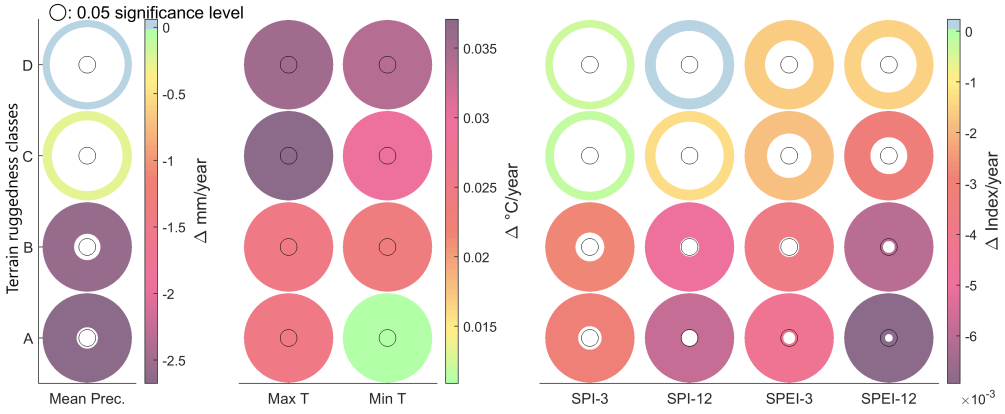

Figure 6. Trend analysis on mean annual precipitation, temperature and drought indices calculated from data belonging to areas defined by terrain ruggedness inside cells. The colour of the circles represents the slope coefficient of the trend, while the inner radius of the circles represents the significance of the trend (a smaller inner radius represents a more significant trend). The black circles denote a significance level of 5%. A, B, C and D areas are displayed in Figure 5g.

even though the temperature reports higher slope coefficients than the other areas. As a comparison, the same trend analysis is performed on data belonging to areas defined by mean elevation thresholds (also defined in Section 2.3) finding largely the same results (not shown here): the two lower mean elevation areas still report significant drying trends for SPEI-12 (but not for SPI-12 and for SPEI-3, the latter being significant only in the second lowest mean elevation area) and no significant precipitation trend, while temperature trends remain significant and with higher coefficients at higher mean elevation areas. Overall, taking the results obtained both with ruggedness-defined areas and with mean elevation-defined areas, a significant difference between the alpine range and the plain area of the domain is observed, the trend analysis reporting worsening drought conditions for the latter.

3.3 Local drought analysis

After analyzing how the general drought conditions in the region have changed over time, the effects of such changes on the characteristics of local drought periods are investigated through a *run analysis* (see Section 3.3). First, the characteristics of local droughts in the region are described as a baseline; then, possible temporal changes in their number, severity, duration and intensity are investigated.

3.3.1 Local droughts characteristics

Despite the differences in observed trends detailed in the previous section, the detection of local droughts by SPI and SPEI shows a high level of correspondence for both 3 and 12 months time scales. After changing each cell's series into a binary series of zeros and ones, where 1 denotes the occurrence of a drought, Cohen's kappa (Cohen, 1960) between the series is calculated as a measure of agreement, with 0 and 1 denoting no agreement and complete agreement respectively. The mean kappa value is slightly higher at 3 month scale (mean kappa equal to 0.86) than at 12 month scale (mean kappa equal to 0.81), but always higher than 0.5: this means that there is always good to excellent agreement between the identification of drought runs based on SPI and on SPEI. Therefore, given that SPI drought runs are based only on precipitation values, it can be stated that a majority of local droughts are determined by precipitation deficits, with temperature itself having a smaller influence on single events, and a greater influence on overall trends (as seen in the comparison between drought indices trends reported in Section 3.2).

In the analysis of local drought characteristics, the longer time scale shows, both for SPI and SPEI, a lower number of runs, but with higher severity (DS_L) and duration (DD_L). Drought intensity (DI_L) values are instead similar between the two time scales, although slightly greater at the 3 month scale. Despite the difference in absolute values, drought analysis indicates a higher number of local droughts, a higher $\overline{DS_L}$ and $\overline{DD_L}$ for SPEI runs compared to SPI runs at both time scales. Thus, when considering both precipitation and ET_0, a greater number of longer and more severe drought periods are detected, compared to the less numerous and shorter periods detected using only precipitation.

One significant difference emerges when comparing the mean drought intensity ($\overline{DI_L}$) values. Average drought intensity is lower for SPEI-3 runs compared to SPI-3, while slightly greater for SPEI-12 compared to SPI-12. This seems to be due to the lower index values reported by SPI-3 compared with SPI-12. The mean negative minimum values during the drought runs are

Table 1. Correlation coefficients (C) and relative p-values between mean drought characteristics and mean elevation, for both SPI and SPEI at 3 an 12 month time scale. Values in italic font denote significant correlation at 5% significance.

	Number of runs		$\overline{\mathbf{DS}}_{\mathbf{L}}$		$\overline{\mathbf{DD}}_{\mathbf{L}}$		$\overline{\mathbf{DI}}_{\mathbf{L}}$	
	C	p-value	C	p-value	C	p-value	C	p-value
SPI-3	*-0.50*	*1.78×10^{-15}*	*-0.35*	*6.60×10^{-8}*	*0.44*	*3.03×10^{-12}*	*0.28*	*2.54×10^{-3}*
SPEI-3	*-0.29*	*7.84×10^{-6}*	*-0.15*	*2.22×10^{-2}*	*0.14*	*3.35×10^{-2}*	-0.05	3.90×10^{-1}
SPI-12	0.06	3.65×10^{-1}	0.13	5.62×10^{-2}	-0.11	9.24×10^{-2}	*0.18*	*6.60×10^{-3}*
SPEI-12	0.04	5.41×10^{-1}	0.05	4.23×10^{-1}	-0.07	3.14×10^{-1}	0.01	9.34×10^{-1}

lower for SPI than for SPEI at both 3 months (-1.65 ± 0.05 for SPI and -1.47 ± 0.03 for SPEI) and 12 months (-1.52 ± 0.07 for SPI and -1.46 ± 0.06 for SPEI) time scales, but, while SPEI values remain almost constant, SPI values show less negative mean minimum values at the longer time scale. This fact, combined with the similarly longer SPEI droughts at both time scales leads to the slightly higher $\overline{\mathrm{DI}}_{\mathrm{L}}$ for SPEI-12.

Regarding the spatial distribution of mean local drought characteristics (number of runs, $\overline{\mathrm{DS}}_{\mathrm{L}}$, $\overline{\mathrm{DD}}_{\mathrm{L}}$ and $\overline{\mathrm{DI}}_{\mathrm{L}}$), SPI and SPEI show similar results when compared at the same time scale, while deviating significantly between 3 and 12 months time scales. SPI-3 and SPEI-3 drought characteristics do not display any spatial gradient, but do display some correlation with mean elevation (Table 1). In particular, when areas at a higher mean elevation are considered, a lower number of more severe, longer and, for SPI-3 only, less intense droughts are reported (although with some differences in the degree of correlation). All together, these results indicate that, on shorter time scales, droughts in higher mean elevation areas tend to be more clustered. Even so, visual inspection of the spatial distribution of local drought characteristics for SPI-3 and SPEI-3 (see supplementary Figure C1) shows that spatial variability of characteristics is overall quite high. Conversely, the higher mean elevation points of the mountainous part of the domain do show quite uniform drought characteristics consistent with the observed correlations, . It can therefore be stated that, despite some significant effects of mean elevation on the characteristics of drought periods, local orography and meteorological conditions play a key role.

SPI-12 and SPEI-12 run characteristics display no spatial gradient (see supplementary Figure C2) and no correlation with mean elevation in terms of number, severity and duration of runs. The only statistically significant correlation found is with SPI-12's $\overline{\mathrm{DI}}_{\mathrm{L}}$, with higher mean elevation areas reporting less intense events, coherent with the results obtained for SPI-3.

Possible correlations of drought characteristics with terrain ruggedness are also considered (Table 2), but the resulting correlation values are always similar or lower than those found with elevation for the 3 month scale, with the only exception being the significant negative correlation between terrain ruggedness and SPEI-3's $\overline{\mathrm{DI}}_{\mathrm{L}}$. Conversely, indices at the 12 month scale reported significant correlations for the number of runs and their $\overline{\mathrm{DS}}_{\mathrm{L}}$ and $\overline{\mathrm{DD}}_{\mathrm{L}}$, with rugged terrain reporting less numerous, less severe and shorter droughts.

Table 2. Correlation coefficients (C) and relative p-values between mean drought characteristics and terrain ruggedness, for both SPI and SPEI at 3 an 12 month time scale. Values in italic font denote significant correlation at 5% significance.

	Number of runs		$\overline{\mathbf{DS}}_{\mathbf{L}}$		$\overline{\mathbf{DD}}_{\mathbf{L}}$		$\overline{\mathbf{DI}}_{\mathbf{L}}$	
	C	p-value	C	p-value	C	p-value	C	p-value
SPI-3	*-0.40*	*6.74×10^{-10}*	*-0.22*	*1.06×10^{-3}*	*0.29*	*7.18×10^{-6}*	*0.21*	*1.13×10^{-4}*
SPEI-3	*-0.22*	*9.87×10^{-4}*	-0.06	3.64×10^{-1}	0.02	7.92×10^{-1}	*-0.23*	*3.26×10^{-4}*
SPI-12	*0.18*	*6.77×10^{-3}*	*0.23*	*3.68×10^{-4}*	*-0.21*	*1.52×10^{-3}*	*0.23*	*6.32×10^{-4}*
SPEI-12	*0.19*	*4.73×10^{-3}*	*0.19*	*3.24×10^{-3}*	*-0.21*	*1.61×10^{-3}*	-0.03	6.25×10^{-1}

3.3.2 Temporal analysis of drought run characteristics

Trend analysis on the obtained local drought characteristics reports only a few cells (always less than 3% of the domain) showing significant trends for drought duration, severity and intensity (DD_L, DS_L and DI_L). In comparison, SPEI-3 shows a far greater amount of cells, slightly more than 10% of the total area, with significant increasing trends for DS_L and DI_L, distributed almost exclusively along the alpine chain, particularly near the southern border (not shown here). The yearly predicted change, in terms of percentage of the relative $\overline{DS}_L/\overline{DI}_L$ for the cell, ranges from 1 to 11% and 0.01 to 1% for severity and intensity respectively.

Despite the overall lack of significant trends, clear differences can be found between the characteristics of drought runs that started before and after 1990, approximately at half the series' length. SPI-3 and SPEI-3 display on average an increase in the number of droughts (more markedly in the case of SPEI-3), and in their DI_L. Opposite results are found in terms of DS_L and DD_L, with SPI-3 indicating a shift towards less severe and shorter droughts, and vice-versa for SPEI-3. Significantly, this difference seems to be caused mainly by cells located in the flat part of the region, where SPEI-3 indicates a shift towards greater DS_L and DD_L (Figure 7a-b). The rest of the region shows similar results for the two indices. The alpine chain, especially in the north, shows a shift towards a higher number of less severe, shorter and less intense droughts. SPI-12 and SPEI-12, on the other hand, report agreeing results and show on average a change towards a lower number of more severe, longer and more intense droughts across the domain. The only exception is the alpine chain, where for a small but continuous area a change towards less numerous, less severe, shorter and less intense droughts is found.

These relative changes are highly correlated with the ruggedness of the area (Table 3). For example, at the 3-month scale, the flat part of the region has seen a change towards less numerous, more severe, longer and more intense droughts, while the alpine chain shows an opposite change. Changes in SPEI-12 run characteristics also display a similar correlation for $\overline{DS}_L$, $\overline{DD}_L$ and $\overline{DI}_L$ but opposite in terms of number of droughts. Therefore, it seems that SPEI-12 droughts got more numerous, more severe, longer and more intense in the lowlands, and, although not quite as strongly, the opposite has happened in the alpine

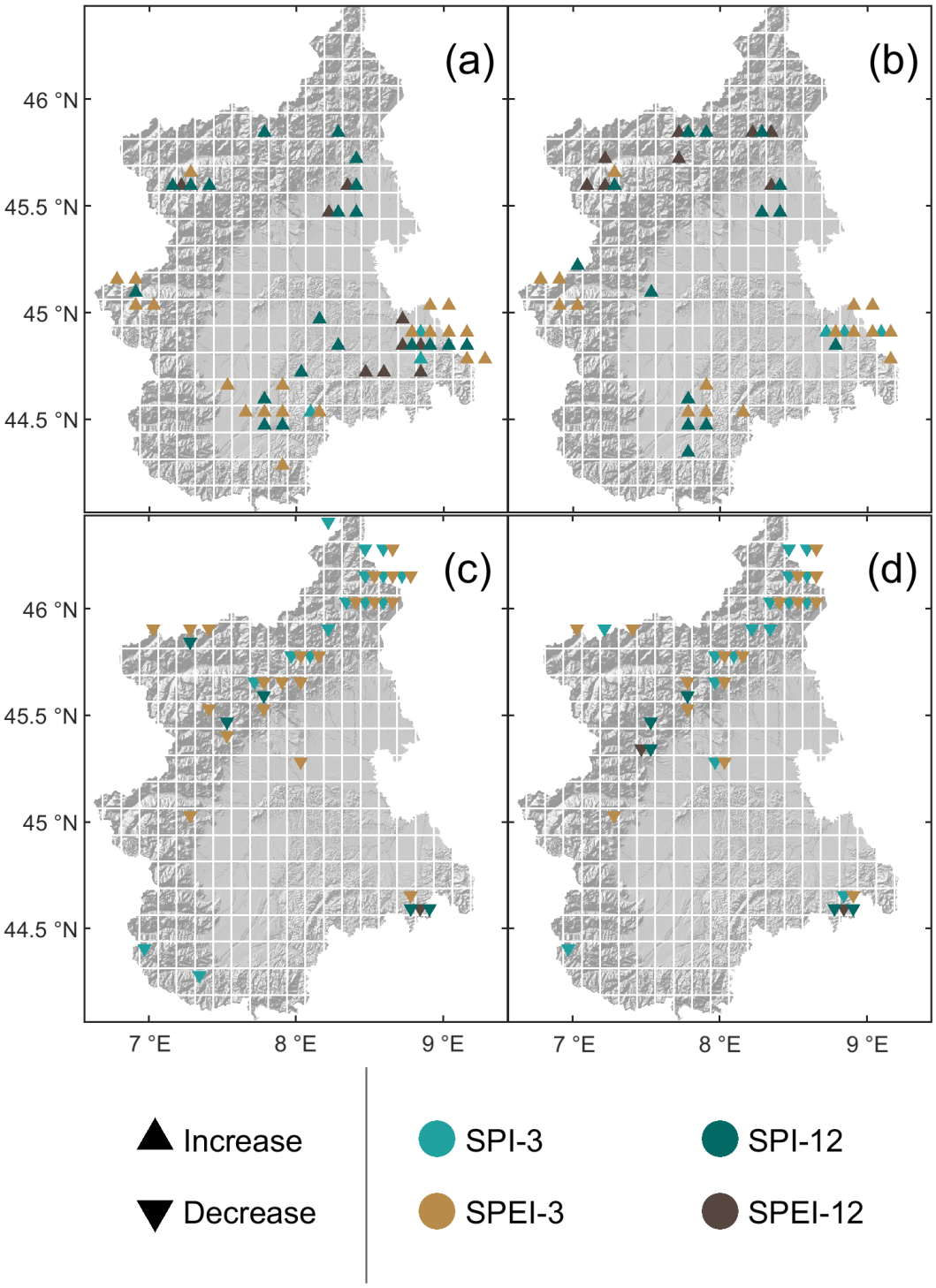

Figure 7. Cells with significant changes in mean drought characteristics between the 1958-1990 and 1990-2023 periods according to the two sample t-test. **(a)** Mean drought severity ($\overline{DS}_L$) increase, **(c)** $\overline{DS}_L$ decrease, **(b)** Mean drought duration ($\overline{DD}_L$) increase, **(d)** $\overline{DD}_L$ decrease.

Table 3. Correlation coefficients (C) and relative p-values between change in mean drought characteristics pre- and post-1990 and terrain ruggedness, for both SPI and SPEI at 3 an 12 month time scale. Values in italic font denote significant correlation at 5% significance.

	ΔNumber of runs		**$\Delta\overline{DS}_L$**		**$\Delta\overline{DD}_L$**		**$\Delta\overline{DI}_L$**	
	C	p-value	C	p-value	C	p-value	C	p-value
SPI-3	*0.18*	*5.22×10^{-3}*	*0.42*	*3.07×10^{-11}*	*-0.37*	*8.66×10^{-9}*	*0.41*	*1.90×10^{-10}*
SPEI-3	*0.23*	*5.57×10^{-4}*	*0.38*	*2.30×10^{-9}*	*-0.38*	*4.11×10^{-9}*	*0.26*	*6.39×10^{-5}*
SPI-12	*-0.33*	*3.18×10^{-7}*	*0.25*	*1.79×10^{-4}*	*-0.27*	*4.94×10^{-5}*	0.09	1.67×10^{-1}
SPEI-12	*-0.25*	*1.70×10^{-4}*	*0.32*	*1.05×10^{-6}*	*-0.30*	*3.95×10^{-6}*	*0.28*	*1.85×10^{-5}*

chain. SPI-12 does show an increase in the number, severity and duration of droughts in the lowlands and a decrease in the mountains, but no correlation for $\overline{DI}_L$.

Changes in local drought characteristics, as opposed to average values, report higher correlation with terrain ruggedness than with mean elevation. Overall, correlation values are also higher than those found for average local drought characteristics, and visual inspection of the spatial distribution (not shown here) does show a quite homogeneous distribution of drought characteristics change between the mountains (especially on the windward side, i.e. the one facing the Po plain) and the plains and hills. The only outliers are the Aosta valley and another valley close to the western border, with changes often in common with the lowlands.

Still, most of the changes found by comparing the two periods are not found to be significant according to the two sample t-test, and thus do not denote a change in the probability distribution of local drought characteristics. The cells with significant changes (reported in Figure 7) are mostly distributed between two areas: changes towards more severe (according to SPI-12, SPEI-3 and SPEI-12), longer (by both indices at the 3 month scale) and more intense (by both indices at the 12 month scale) droughts are reported for the eastern-most part of the domain; changes towards less severe and shorter droughts are reported mostly in the northern part of the alpine chain for SPI/SPEI at the 3 month scale, while almost no significant shifts towards less intense local droughts are reported.

3.4 Region-wide drought event analysis

This section introduces the results obtained from the analysis of region wide drought events (see Section 3.4). Similarly to the previous section, both the characteristics of drought events and their change over time are discussed.

3.4.1 Drought event characteristics

Region-wide drought events are calculated from SPI and SPEI index series at 3 and 12 month scale. The analysis displays similar results between the two indices at the same time scale, with all main events identified by both SPI and SPEI, and high agreement between the extent of the area in drought conditions over time.

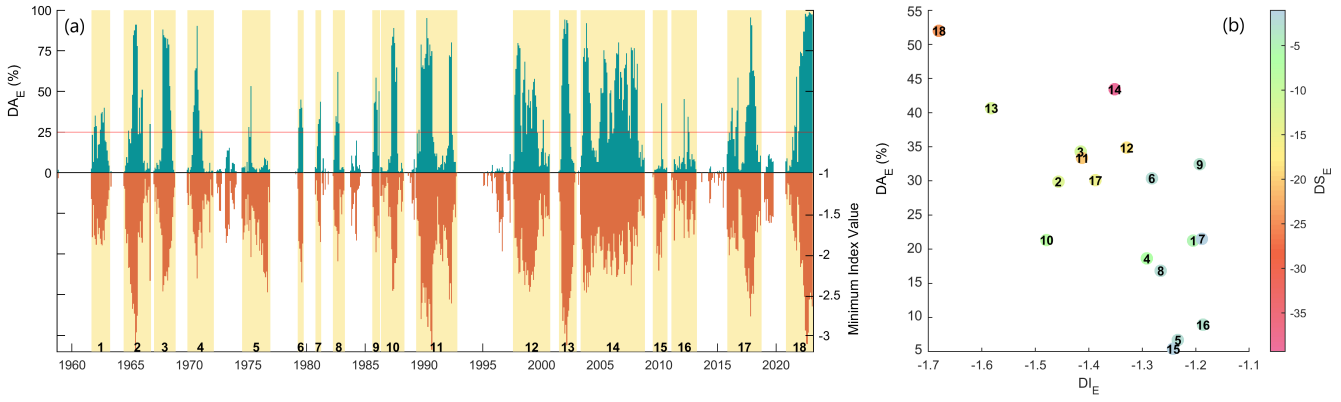

Figure 8. Region-wide drought event analysis conducted on SPEI-12. **(a)** Time series of percentage of cells in drought condition (only the portion below the -1 threshold, upper part of the diagram) and minimum index value in the domain (lower part of the diagram). Each event is highlighted in yellow and labeled. **(b)** Drought event characteristics: drought intensity (DI_E), mean drought area (DA_E) and drought severity (DS_E).

The analysis at the 3 month scale reports about 60 events (see supplementary Figure D1), while the analysis at the 12 month scale (for SPEI-12 see Figure 8, for SPI-12 see supplementary Figure D2) reports less than 20. Region-wide drought events at the longer time scale are also far more severe and longer than those at the shorter time scale, but intensity and area values are similar. Regarding relative differences between the drought characteristics between SPI and SPEI at both time scales, $\overline{DS}_E$ is similar between the two indices , $\overline{DD}_E$ is higher for SPEI, and both $\overline{DI}_E$ and $\overline{DA}_E$ are higher for SPI. On the other hand, when considering the mean highest area affected by drought conditions in every single event both indices report similar results at both time scales. Overall, this indicates that the same deficit tends to affect a slightly wider area, with a higher intensity but for less time when only precipitation is considered, while it tends to affect the same overall area with less intensity and for a longer time when both precipitation and temperature are considered.

Region-wide drought event analysis on SPI-12 and SPEI-12 was also useful in indicating the main drought events that happened in the region in the last 60 years. Of these, the last one, starting in the winter of 2021 and still ongoing, was identified as perhaps the most extreme in the series. In particular, the wide area affected by drought during this event and its severity, second only to the longest 2001-2008 event, mark it as an exceptional drought for the region. The intensity value is also the highest of all detected events, but this may not be significant given that this last event has not yet ended. Certainly, the fact that its severity is higher than the severity of the 2001-2002 event as detected through SPEI-12, also adds to how exceptional this last event is.

Table 4. Drought event characteristics before and after 1990. Values in italic font font denote significant differences between the two distributions at 5% significance.

	Number of events		$\overline{\mathbf{DS_E}}$		$\overline{\mathbf{DD_E}}$ **(months)**		$\overline{\mathbf{DI_E}}$		$\overline{\mathbf{DA_E}}$ **(%)**	
	Pre 1990	Post 1990	Pre 1990	Post 1990	Pre 1990	Post 1990	Pre 1990	Post 1990	Pre 1990	Post 1990
SPI-3	31	28	-3.24	-3.30	5.68	5.90	-1.45	-1.50	38.51	35.13
SPEI-3	27	32	-3.10	-3.40	6.18	6.56	-1.32	-1.36	37.50	32.05
SPI-12	12	5	*-7.14*	*-19.34*	*14.33*	*36.60*	-1.37	-1.42	31.61	32.05
SPEI-12	11	7	-6.92	-16.14	20.27	32.28	-1.31	-1.39	24.24	30.77

3.4.2 Temporal analysis of drought event characteristics

Trend analysis reports no significant results for the drought characteristics of region-wide drought events. Confronting the values before and after 1990 does show results consistent with those found for local droughts (Table 4): drought events have become more severe, longer and more intense at both time scales. Also similar to drought runs, the number of drought events has increased at the shorter 3 month time scale while it has decreased at the longer 12 month scale. Another difference is in the $\overline{\mathrm{DA}}_{\mathrm{E}}$, which has decreased at the 3 month time scale and has increased at the 12 month time scale. Overall, this seems to indicate that, on a region wide level, drought conditions have worsened between the periods 1960-1990 and 1990-2000, with short term deficits becoming more common over slightly smaller areas, leading to more generalised deficits over wider areas at the longer time scales. Despite many of the described changes not being significant according to the two sample t-test, $\overline{\mathrm{DS}}_{\mathrm{E}}$ and $\overline{\mathrm{DD}}_{\mathrm{E}}$ for SPI-12 do report a statistically significant shift in the mean before and after 1990. Changes in $\overline{\mathrm{DS}}_{\mathrm{E}}$ and $\overline{\mathrm{DD}}_{\mathrm{E}}$ for SPEI-12 also report p-values close to the 5% level, although not falling below the 5% threshold. This seems to confirm that the shift towards worse region-wide drought conditions (higher severity and longer duration) is more evident at longer time scales, and that this shift is mainly caused by a change in precipitation patterns.

Despite the apparent importance of precipitation, the only significant trend in terms of the percentage of the domain in drought conditions (index lower than -1) over time is found for SPEI-12, with a slope coefficient of 2.92×10^{-4}/year .

4 Discussion and conclusion

In this study, 60 years of precipitation and temperature data are analyzed in order to characterise changes in drought conditions in the Piedmont and Aosta valley area, reaching the following conclusions:

1. Trend analysis on temperature and precipitation indicates the presence of a widespread temperature increase in the region—despite occasional different results considering minimum and maximum temperatures—while few precipitation trends are found. Precipitation changes are largely related to season, with clear differences between the winter months

(with uniform decreases of precipitation) and the rest of the year, and seem to affect only small portions of the territory, not leading to a region-wide significant trend.

2. Evidence of widespread drying trends in the region is found through the trend analysis of SPI and SPEI series. Temperature plays a key role in defining these drying trends, as the SPEI reports negative trends for wider areas and with greater slope coefficients than SPI. Still, the areas showing the more severe drying trends do not coincide with the areas showing the highest warming rates, indicating that changes in droughts are governed by the interplay between temperature and precipitation.

3. The start and end of single drought periods seem to be mainly determined by precipitation anomalies, in contrast to the importance of temperature in determining long-term conditions. Both local and region-wide drought periods are identified by both SPI and SPEI, meaning that temperature alone does not seem to be able to determine drought conditions in the absence of precipitation deficits.

4. Some evidence of an increase in the severity, duration and intensity of drought periods after 1990 is found, although often not statistically significant. A tendency for drought periods at 3 month time scale to become more numerous, and for drought periods at 12 month time scale to become less numerous is observed, both at a local and regional scale. Thus, while the percentage of time under drought conditions has become greater at both time scales, it seems that a larger amount of short-term deficits aggregate into long-term deficits with higher duration. In addition to this, a significant positive trend in the percentage of the area under drought conditions according to SPEI-12 is detected.

5. Changes in the characteristics of local drought periods are affected by temperature increase, as drought periods obtained from SPEI series show more pronounced increases in severity, duration and intensity than those obtained from SPI series. Contrary to this, drought events at a region-wide scale show more marked shifts in severity and duration for SPI than for SPEI, denoting a more significant influence of regional precipitation patterns than of temperature on droughts at a regional scale.

6. Terrain characteristics and mean elevation show significant influence on the observed trends and changes in drought characteristics, with drying trends being more severe the lower and less rugged the area. In fact, when the mountainous parts and the flat part of the domain are considered separately, the first shows no significant drought trends, while the second reports significant drying trends for both SPI and SPEI at multiple timescales. In the case of drought period characteristics, decreases in their severity, duration and intensity are mostly found in the alpine range, while increases are mostly found in the smoother and low lying areas.

The results presented are coherent with previous studies conducted in the same study-area (presented in Section 1) in regards to the role of temperature as a consistent driver of drought increase. On the other hand, no unanimous result regarding the presence and seasonality of precipitation change can be determined from the presented studies. Our analysis only agrees with those finding a non-significant annual trend and a negative winter trend for precipitation values. Still, despite the worsening

of drought conditions related to precipitation and temperature being clear, how these changes may affect the characteristics of single drought periods remains less clear. Statistically significant changes in local drought characteristics between the two halves of the analysed series are found, but almost no significant trends could be detected. As such, it is difficult to asses whether the increase in severity, duration and intensity of drought periods is actually part of a general tendency, that would be coherent with the detected worsening drought conditions, and is not just determined by the extreme drought events present in the second half of the series; .

On a more local scale, the higher resolution of the analyzed data, compared to previous studies, makes it possible to show quite dishomogeneous results regarding the presence of drying/wetting trends, as well as drought characteristics, in different portions of the region. As a possible explanation of this result, our analysis studies relations between terrain characteristics and drought characteristics, finding several significant correlations. This type of analysis is in common with a growing body of literature focused on the elevation effects on drought characteristics, with studies conducted in the Qinghai–Tibet plateau (Feng et al., 2020), the Lorestan province in Iran (Hosseini et al., 2020), the Indus river basin (Dubey et al., 2023) and the Canary Islands (Carrillo et al., 2023). These studies, using mean elevation as a topographic variable, find different results in regards to the distribution of drought trends at high/low elevations, and as such no general claim about the tendency of different elevation areas to show drying/wetting trends can be made. Thus, our finding of more severe drying trends and worsening drought characteristics in the lower altitude part of the region can only be interpreted as a further proof of the importance of considering topographic effects in areas with highly diverse terrain. More importantly, our study shows that mean elevation, although certainly a variable to be considered, shouldn't be the only topographic variable taken into account. For example, here we propose the use of a simple terrain ruggedness measure to capture different terrain characteristics of the domain: in our case, this metric was chosen in order to distinguish a low-lying flat portion of the domain from a low-lying hilly portion, despite similar mean elevation of the corresponding cells. In our analysis, using this different classification leads to stronger correlations between drought characteristics and topographical characteristics, particularly regarding drought trends and changes in local droughts characteristics.

Although strong correlations between drought trends and the mean elevation and ruggedness of the terrain are found, attribution of these results to physical phenomena is not straightforward. The presented methodology doesn't focus on this aspect and, given the complexity of the involved phenomena, attribution is outside the scope of our study. However, our finding of different meteorological conditions between the alpine chain and the surrounding Po plain is consistent with other studies concerning the presence of an increase in alpine summer convective precipitation not in common with the surrounding areas (Giorgi et al., 2016; Grose et al., 2019). In this study we restrict our focus to near-past and current conditions and do not consider predictions of future conditions (although strong drying trends in some portions of the study area are detected). Further research is needed to study how the drought characteristics of areas at different elevations and with different reliefs may evolve under climate change. Still, the results presented in this paper can be useful inputs regarding the analysis of soil moisture and hydrological droughts in the Piedmont and Aosta valley region, showing the need to consider areas with distinct topographical features as well as giving an indication of which areas are more likely to face dryer conditions.

Data availability. The data that support the findings of this study are openly available in the NWIOI data set at https://www.arpa.piemonte.it/rischinaturali/t
storici/dati/dati.html, maintained and updated by the Forecast Systems Department of the Regional Environmental Protection Agency of
515 Piedmont (*Dipartimento Sistemi Previsionali - Arpa Piemonte*).

Appendix A: Optimal Interpolation Method

As discussed in Section 2.2, the Optimal Interpolation Method was used by *Arpa Piemonte* to develop the NWIOI dataset used in the present work. The analysis method is described in detail in Uboldi et al. (2008), but information regarding the specific choices made for the dataset are reported in the following paragraphs.

The method produces a regular grid of data by interpolating the station data at each time step. In particular, the interpolation is done by modifying a previously obtained *background* or *first-guess* field available at the desired grid points via a linear relation with the *innovation vector*, meaning the difference between the observed values and the background field values at station points:

$$x_a = x_b + K(y_0 - y_b) \tag{A1}$$

where the vector x_a contains the interpolated (or analyzed) values at each grid node, the vector x_b contains the background field values at each grid point, the vector y_0 contains the observed values at each station point and the vector y_b contains the background field values at each station point. The matrix K is called the gain matrix and is estimated using the three parameters that act similarly to cut-off wavelengths of a low pass filter. The three parameters are proportional to the confidence in the observation data over the background field and the size of the horizontal and vertical "influence area" of each station. Given a certain distribution of station points, the three parameters are thus chosen by first evaluating the *integral data influence* field, meaning the x_a values obtained when all background field values are set to 0 and all station values are set to 1. Calibration of the parameters aims at creating an integral data influence field as uniform and as close to 1 as possible. Given that the number of available stations has changed throughout the series (from 25 to 371 and from 119 to 386 for temperature and precipitation stations respectively), the parameters needed for the calculation of the K matrix were chosen on a year-by-year basis.

The described interpolation method was applied to both temperature and precipitation data, using two different background fields and calculating two different sets of parameters for each year. For the temperature interpolation, the reanalysis set ERA-40 (Kållberg et al., 2004) published by the European Centre for Medium Range Weather Forecast (ECMWF) for the 1957-2001 period and, for the following period, ECMWF analyses' set were used as background fields. For the precipitation no external background field was used, instead calculating a pseudo-background field from the station data itself via linear function of the spatial coordinates by performing a least-square minimization (Uboldi et al., 2008). Furthermore, the interpolation of the precipitation data was rendered two-dimensional by assigning the same elevation to each station point (temperature interpolation was instead three-dimensional) due to considerations about the high variability of conditions inside each cell, particularly in the alpine area.

Finally, minor editing is applied to the already analyzed and validated data: a small percentage (slightly under 1%) of data reports the maximum daily temperature as lower than the minimum daily temperature. Given that the data set is used to calculate monthly means, such data is discarded.

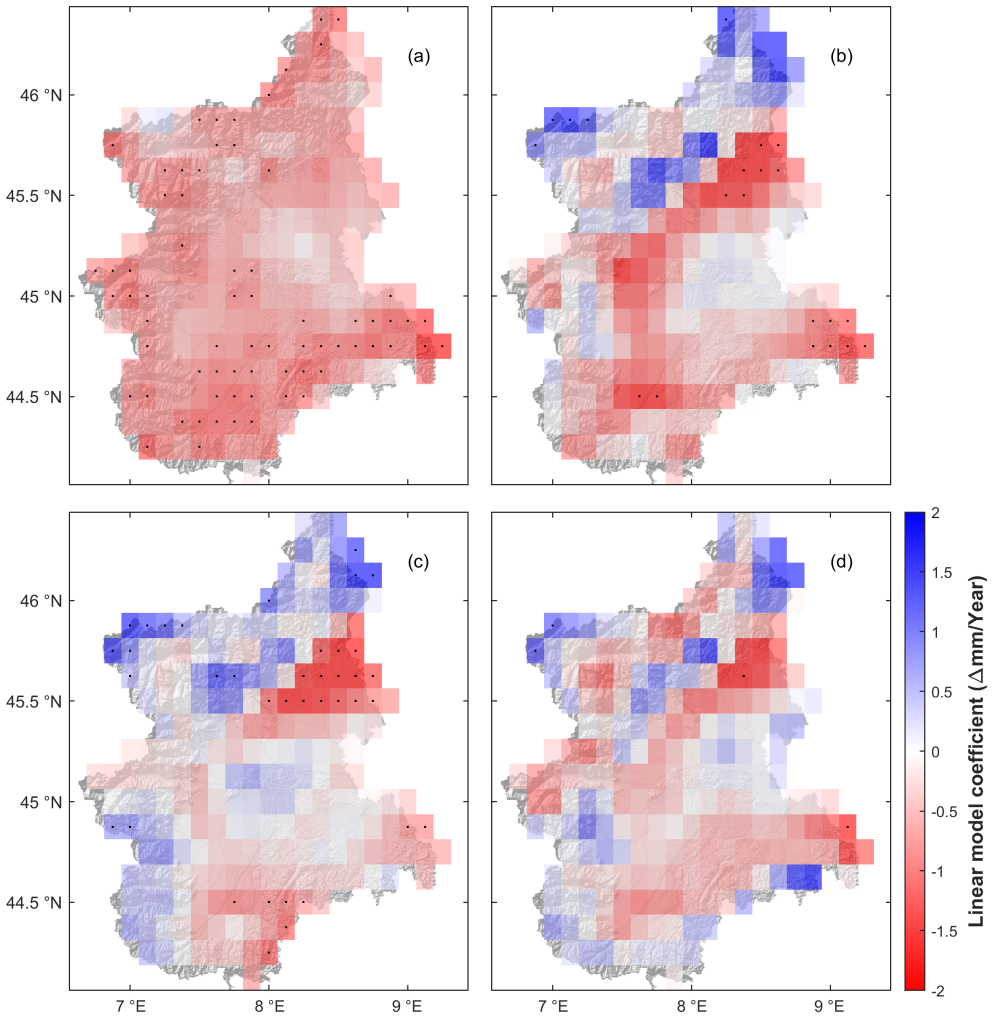

Figure B1. Seasonal trend analysis on monthly precipitation values. **(a)** Winter, **(b)** Spring, **(c)** Summer, **(d)** Autumn. Cells containing a dot denote significant trends at 5% significance.

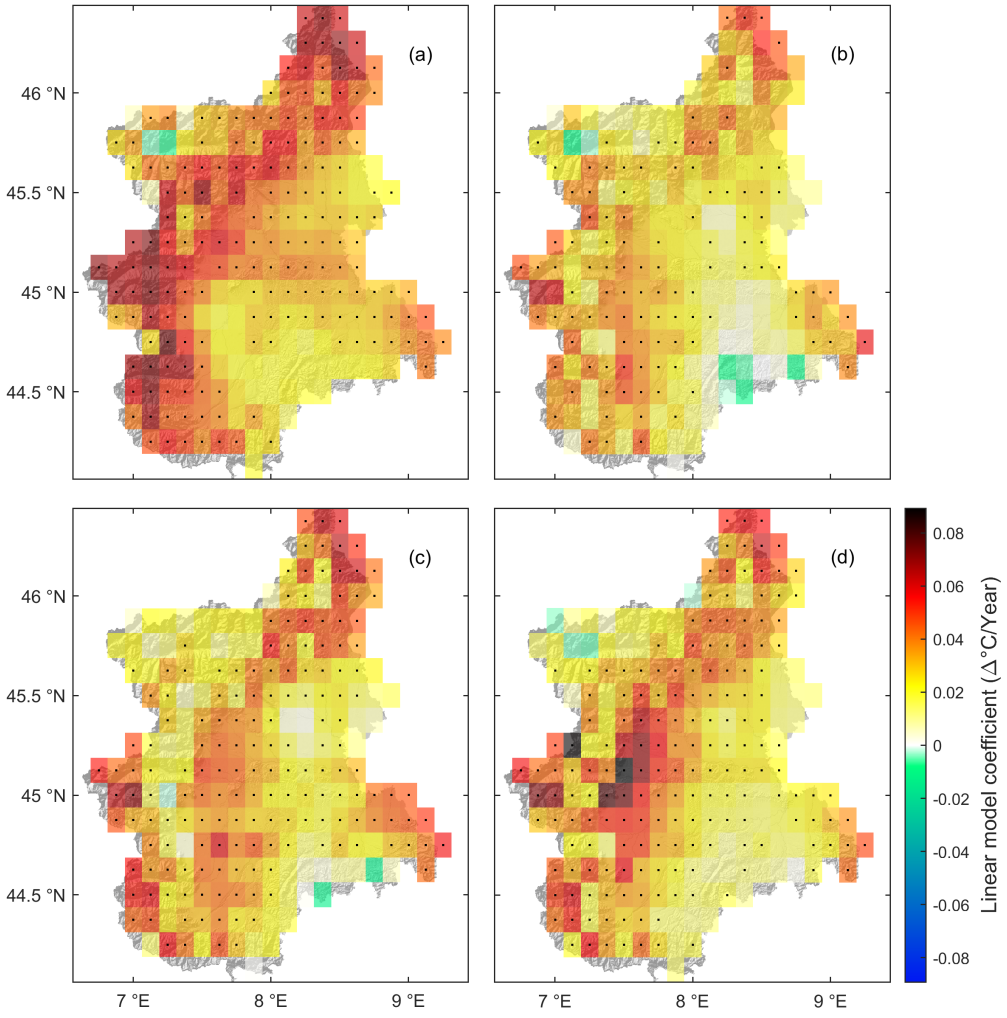

Figure B2. Seasonal trend analysis on monthly maximum temperature values. **(a)** Winter, **(b)** Spring, **(c)** Summer, **(d)** Autumn. Cells containing a dot denote significant trends at 5% significance.

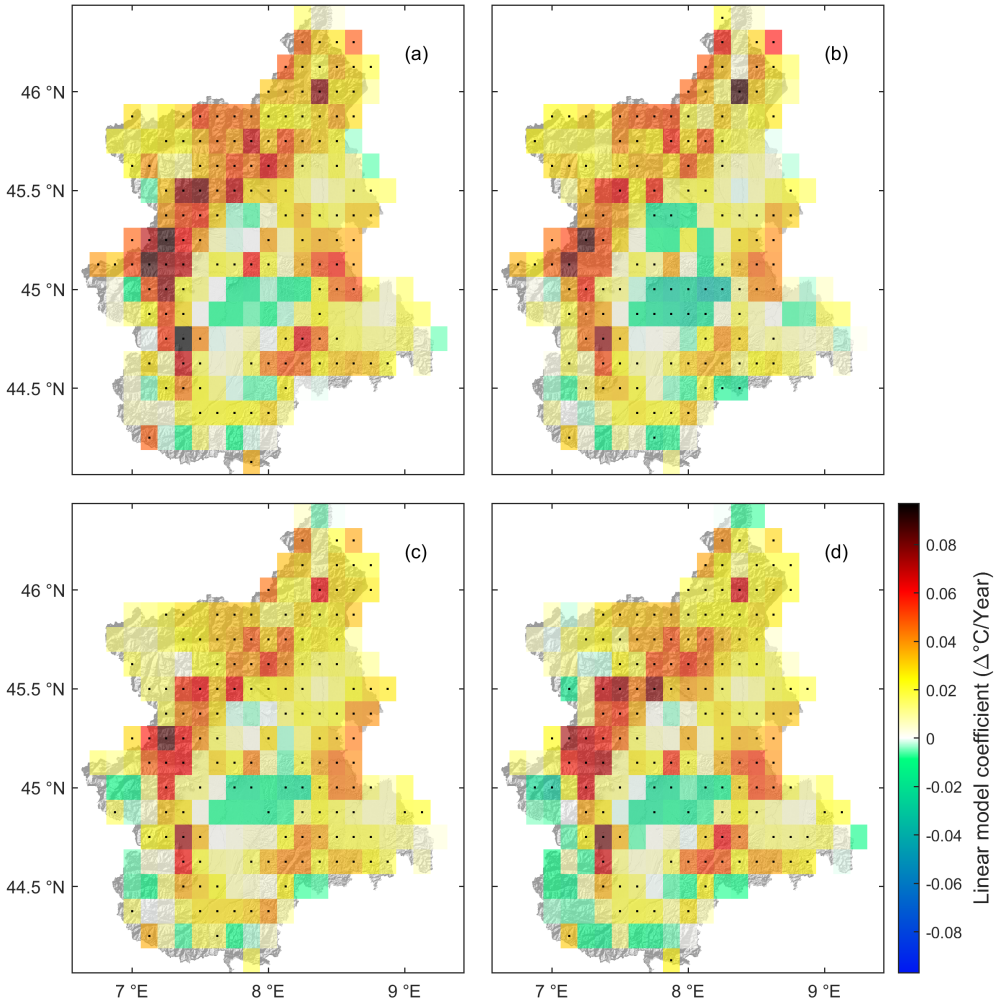

Figure B3. Seasonal trend analysis on monthly minimum temperature values. **(a)** Winter, **(b)** Spring, **(c)** Summer, **(d)** Autumn. Cells containing a dot denote significant trends at 5% significance.

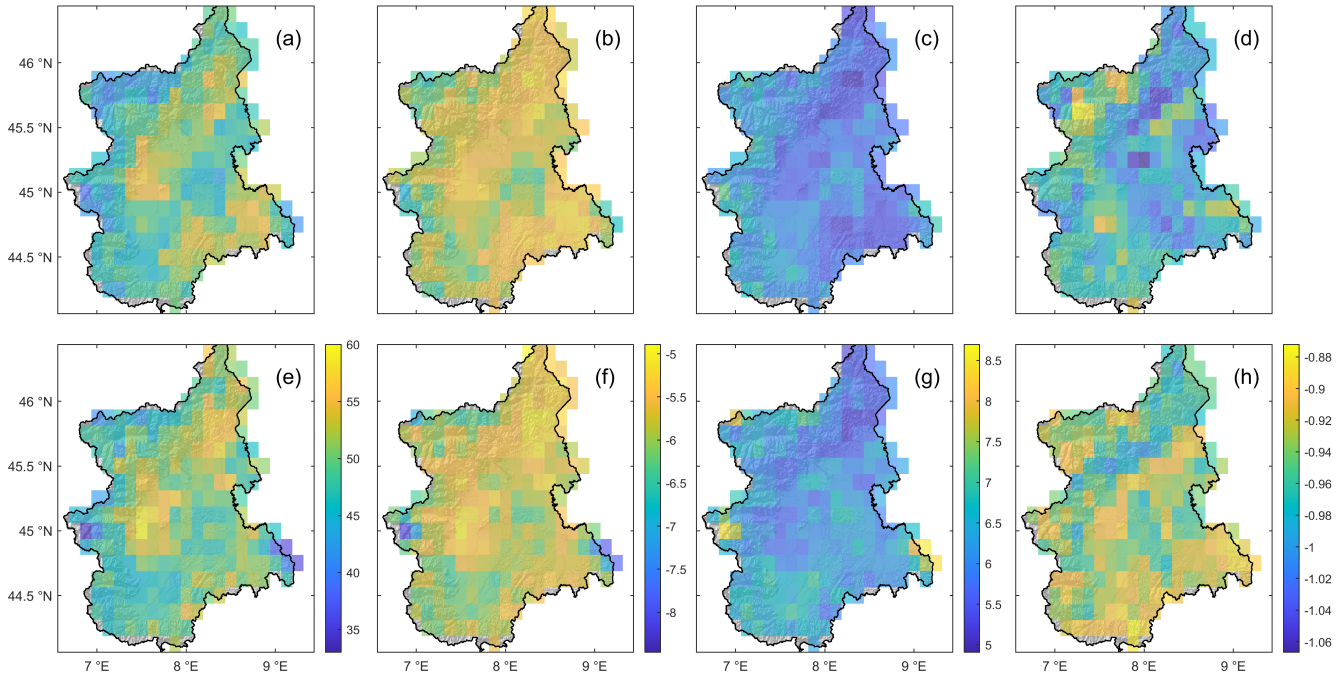

Figure C1. Spatial distribution of drought run characteristics at 3 month time scale. SPI-3's number of runs **(a)**, average severity of local drought $\overline{\mathrm{DS}}_{\mathrm{L}}$ **(b)**, average length of local drought $\overline{\mathrm{DD}}_{\mathrm{L}}$ **(c)**, average intensity of local drought $\overline{\mathrm{DI}}_{\mathrm{L}}$ **(d)**. SPEI-3's number of runs **(e)**, $\overline{\mathrm{DS}}_{\mathrm{L}}$ **(f)**, $\overline{\mathrm{DD}}_{\mathrm{L}}$ **(g)**, $\overline{\mathrm{DI}}_{\mathrm{L}}$ **(h)**.

Appendix B: Trend analysis on seasonal precipitation and temperature values

As discussed in Section 3.3.1, trend analysis is conducted on monthly precipitation and maximum/minimum temperatures on both an annual and seasonal scale. Seasons are defined as the three month periods December-January-February (Winter), March-April-May (Spring), June-July-August (Summer), September-October-November (Fall). Results for the seasonal trend analysis of monthly precipitations are reported in Figure B1; results for the seasonal trend analysis of monthly maximum temperatures are reported in Figure B2; results for the seasonal trend analysis of monthly maximum temperatures are reported in Figure B3

Appendix C: Spatial distribution of drought run characteristics

As discussed in section 3.3.1, the spatial distribution of drought run characteristics is analyzed, particularly in its correlation with mean elevation/terrain ruggedness. Maps of the spatial distribution of drought characteristics are shown for SPI-3 and SPEI-3 in Figure C1, and for SPI-12 and SPEI-12 in Figure C2.

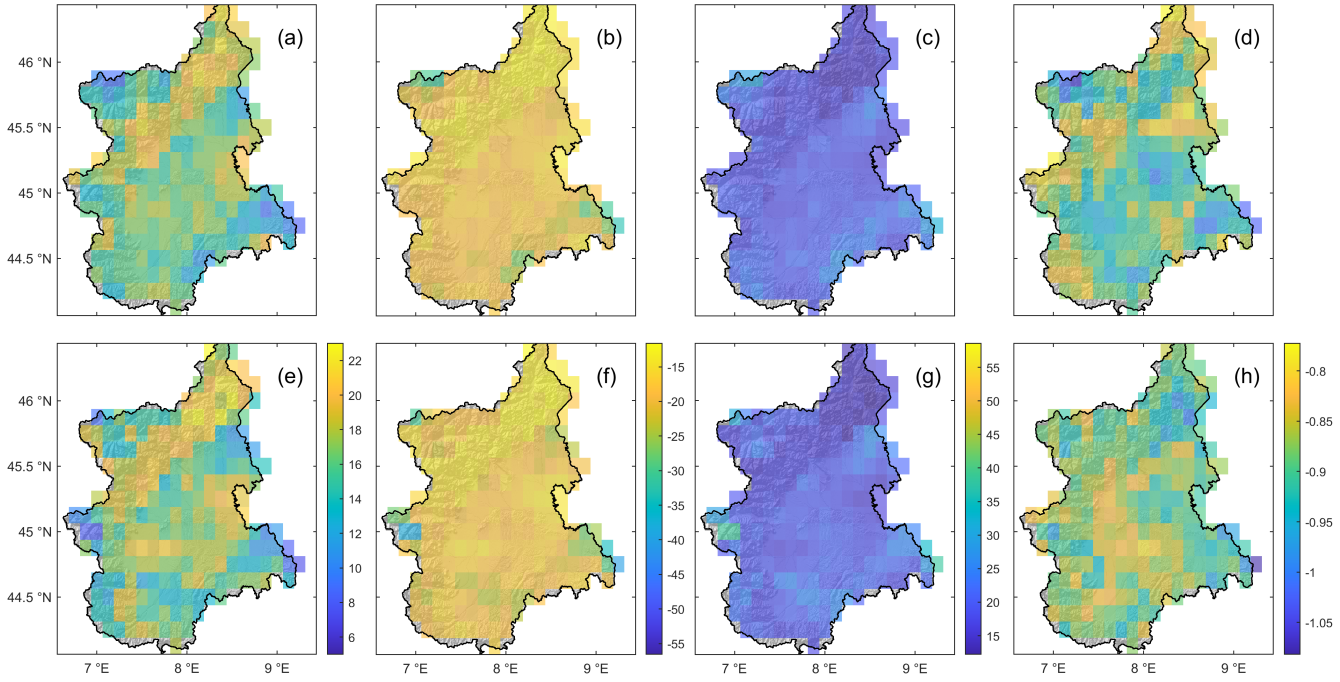

Figure C2. Spatial distribution of drought run characteristics at 12 month time scale. SPI-12's number of runs **(a)**, average severity of local drought $\overline{DS}_L$ **(b)**, average length of local drought $\overline{DD}_L$ **(c)**, average intensity of local drought $\overline{DI}_L$ **(d)**. SPEI-12's number of runs **(e)**, $\overline{DS}_L$ **(f)**, $\overline{DD}_L$ **(g)**, $\overline{DI}_L$ **(h)**.

Appendix D: Region-wide drought event analysis

As discussed in Section 3.4, region-wide drought analysis is conducted on SPI and SPEI at 3 and 12 month scales. The results for SPI-3 and SPEI-3 are shown in Figure D1, the results for SPI-12 are shown in Figure D2.

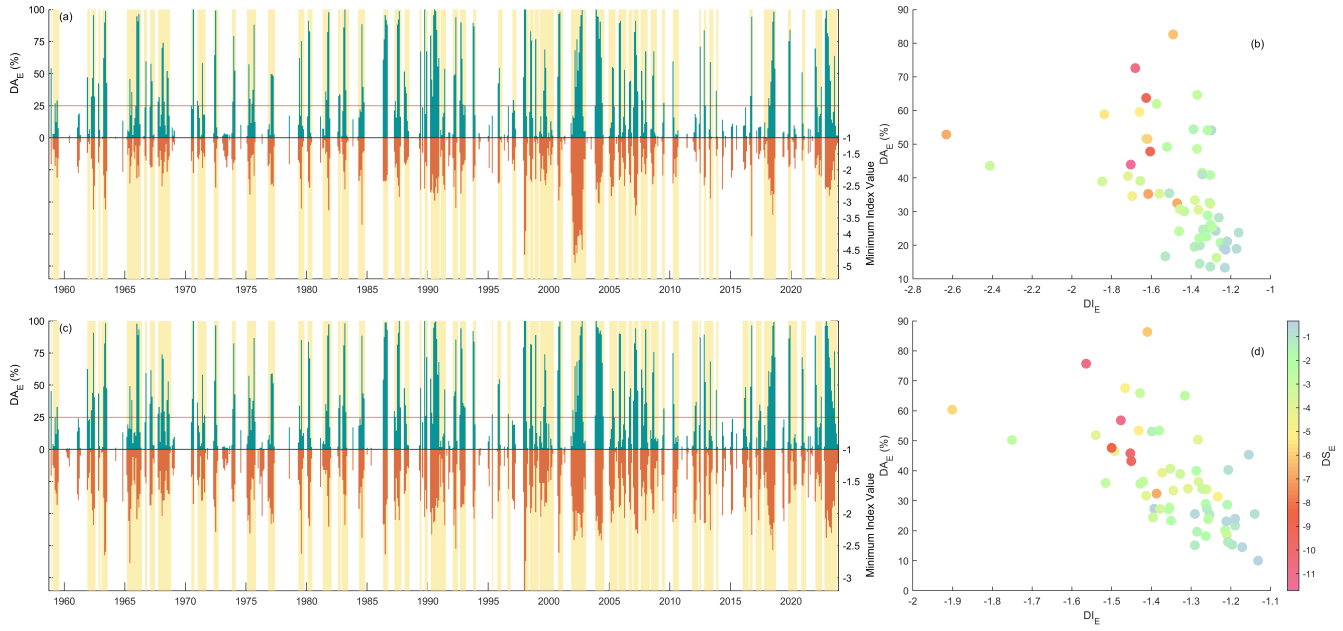

Figure D1. Region-wide drought event analysis conducted on the indices at 3 month scale. **(a)** Series of percentage of cells in drought condition (below the -1 threshold) and the minimum index value in the domain for SPI-3. **(b)** Drought event characteristics for SPI-3. **(c)** Series of percentage of cells in drought condition (below the -1 threshold) and the minimum index value in the domain for SPEI-3. **(d)** Drought event characteristics for SPEI-3.

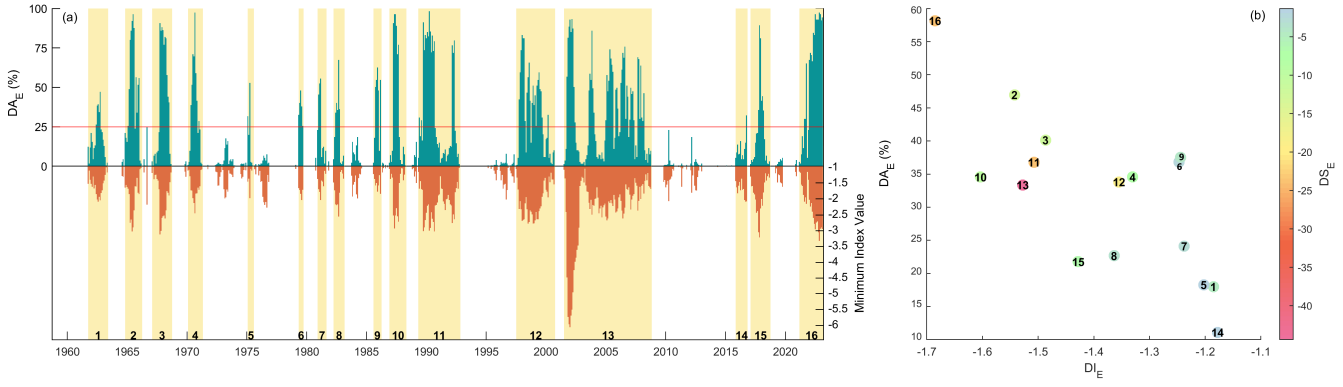

Figure D2. Region-wide drought event analysis conducted on SPI-12. **(a)** Series of percentage of cells in drought condition (below the -1 threshold) and the minimum index value in the domain. Each event is highlighted in yellow and labeled. **(b)** Drought event characteristics.

Author contributions. M.E., S.T., A.V. and R.R. contributed to the design of the research, to the analysis of the results and to the writing of the manuscript. M.E. carried out the analysis.

Competing interests. The authors declare no competing interests.

Acknowledgements. This study was carried out within the RETURN Extended Partnership and received funding from the European Union Next-GenerationEU (National Recovery and Resilience Plan – NRRP, Mission 4, Component 2, Investment 1.3 – D.D. 1243 2/8/2022, PE0000005).

References

Acquaotta, F., Fratianni, S., Cassardo, C., and Cremonini, R.: On the continuity and climatic variability of the meteorological stations in Torino, Asti, Vercelli and Oropa, Meteorology and Atmospheric Physics, 103, 279–287, https://doi.org/10.1007/s00703-008-0333-4, 2009.

Acquaotta, F., Fratianni, S., and Garzena, D.: Temperature changes in the North-Western Italian Alps from 1961 to 2010, Theoretical and Applied Climatology, 122, 619–634, https://doi.org/10.1007/s00704-014-1316-7, 2015.

Angelidis, P., Maris, F., Kotsovinos, N., and Hrissanthou, V.: Computation of Drought Index SPI with Alternative Distribution Functions, Water Resources Management, 26, 2453–2473, https://doi.org/10.1007/s11269-012-0026-0, number: 9, 2012.

Arpa Piemonte: Il Piemonte nel Cambiamento Climatico, http://www.arpa.piemonte.it/pubblicazioni-2/pubblicazioni-anno-2007/pdf-il-piemonte-nel-cambiamento-climatico, 2007.

Arpa Piemonte, D. R. N. e. A. e. D. S. P. and Regione Piemonte, Energia e Territorio Settore Progettazione Strategica e Green Economy, D. A.: Analisi del clima regionale del periodo 1981-2010 e tendenze negli ultimi 60 anni, https://www.regione.piemonte.it/web/sites/default/files/media/documenti/2021-02/analisi_clima_regionale_1981-2010.pdf, 2020a.

Arpa Piemonte, D. R. N. e. A. e. D. S. P. and Regione Piemonte, Energia e Territorio Settore Progettazione Strategica e Green Economy, D. A.: Analisi degli scenari di clima regionale del periodo 2011- 2100, https://www.regione.piemonte.it/web/sites/default/files/media/documenti/2021-02/analisi_scenari_clima_regionale_periodo_2011-_2100.pdf, 2020b.

Arpa Piemonte, Dipartimento Sistemi Provisionali: NWIOI Dataset, https://www.arpa.piemonte.it/rischinaturali/tematismi/clima/confronti-storici/dati/dati.html, last acces: 12 February 2024, 2011.

Baronetti, A., González-Hidalgo, J. C., Vicente-Serrano, S. M., Acquaotta, F., and Fratianni, S.: A weekly spatio-temporal distribution of drought events over the Po Plain (North Italy) in the last five decades, International Journal of Climatology, 40, 4463–4476, https://doi.org/10.1002/joc.6467, number: 10, 2020.

Baronetti, A., Dubreuil, V., Provenzale, A., and Fratianni, S.: Future droughts in northern Italy: high-resolution projections using EURO-CORDEX and MED-CORDEX ensembles, Climatic Change, 172, 22, https://doi.org/10.1007/s10584-022-03370-7, 2022.

Beguería, S., Vicente-Serrano, S. M., Reig, F., and Latorre, B.: Standardized precipitation evapotranspiration index (SPEI) revisited: parameter fitting, evapotranspiration models, tools, datasets and drought monitoring, International Journal of Climatology, 34, 3001–3023, https://doi.org/10.1002/joc.3887, number: 10, 2014.

Bordi, I. and Sutera, A.: An analysis of drought in Italy in the last fifty years, Il Nuovo Cimento C, 25, 2002.

Brunetti, M., Maugeri, M., Nanni, T., and Navarra, A.: Droughts and extreme events in regional daily Italian precipitation series, International Journal of Climatology, 22, 543–558, https://doi.org/10.1002/joc.751, number: 5, 2002.

Burek, P., Satoh, Y., Fischer, G. W., Kahil, M. T., Scherzer, A., Tramberend, S., Nava, L. F., Wada, Y., Eisner, S., Flörke, M., Hanasaki, N., Magnuszewski, P., Cosgrove, B., and Wiberg, D.: Water Futures and Solution - Fast Track Initiative (Final Report), 2016.

Caloiero, T., Caroletti, G. N., and Coscarelli, R.: IMERG-Based Meteorological Drought Analysis over Italy, Climate, 9, 65, https://doi.org/10.3390/cli9040065, number: 4, 2021.

Carrillo, J., Hernández-Barrera, S., Expósito, F. J., Díaz, J. P., González, A., and Pérez, J. C.: The uneven impact of climate change on drought with elevation in the Canary Islands, npj Climate and Atmospheric Science, 6, 31, https://doi.org/10.1038/s41612-023-00358-7, 2023.

Choi, S. C. and Wette, R.: Maximum Likelihood Estimation of the Parameters of the Gamma Distribution and Their Bias, Technometrics, 11, 683–690, https://doi.org/10.1080/00401706.1969.10490731, 1969.

Ciccarelli, N., Von Hardenberg, J., Provenzale, A., Ronchi, C., Vargiu, A., and Pelosini, R.: Climate variability in north-western Italy during the second half of the 20th century, Global and Planetary Change, 63, 185–195, https://doi.org/10.1016/j.gloplacha.2008.03.006, 2008.

Cohen, J.: A Coefficient of Agreement for Nominal Scales, Educational and Psychological Measurement, 20, 37–46, https://doi.org/10.1177/001316446002000104, 1960.

Collaud Coen, M., Andrews, E., Bigi, A., Martucci, G., Romanens, G., Vogt, F. P. A., and Vuilleumier, L.: Effects of the prewhitening method, the time granularity, and the time segmentation on the Mann–Kendall trend detection and the associated Sen's slope, Atmospheric Measurement Techniques, 13, 6945–6964, https://doi.org/10.5194/amt-13-6945-2020, 2020.

Crausbay, S. D., Betancourt, J., Bradford, J., Cartwright, J., Dennison, W. C., Dunham, J., Enquist, C. A., Frazier, A. G., Hall, K. R., Littell, J. S., Luce, C. H., Palmer, R., Ramirez, A. R., Rangwala, I., Thompson, L., Walsh, B. M., and Carter, S.: Unfamiliar Territory: Emerging Themes for Ecological Drought Research and Management, One Earth, 3, 337–353, https://doi.org/10.1016/j.oneear.2020.08.019, number: 3, 2020.

Dai, A.: Drought under global warming: a review, WIREs Climate Change, 2, 45–65, https://doi.org/10.1002/wcc.81, 2011.

Dai, A.: Increasing drought under global warming in observations and models, Nature Climate Change, 3, 52–58, https://doi.org/10.1038/nclimate1633, 2013.

Dubey, A., Swami, D., Gupta, V., and Joshi, N.: From the peaks to the plains: Investigating the role of elevation in governing drought dynamics over the Indus river basin, Atmospheric Research, 291, 106 824, https://doi.org/10.1016/j.atmosres.2023.106824, 2023.

Falzoi, S., Acquaotta, F., Pulina, M. A., and Fratianni, S.: Hydrological drought analysis in Continental Temperate and Mediterranean environment during the period 1981-2017, Italian Journal of Agrometeorology, pp. 13–23 Pages, https://doi.org/10.13128/IJAM-798, artwork Size: 13-23 Pages Publisher: Italian Journal of Agrometeorology, 2019.

Feng, W., Lu, H., Yao, T., and Yu, Q.: Drought characteristics and its elevation dependence in the Qinghai–Tibet plateau during the last half-century, Scientific Reports, 10, 14 323, https://doi.org/10.1038/s41598-020-71295-1, 2020.

García-León, D., Standardi, G., and Staccione, A.: An integrated approach for the estimation of agricultural drought costs, Land Use Policy, 100, 104 923, https://doi.org/10.1016/j.landusepol.2020.104923, 2021.

Giorgi, F., Torma, C., Coppola, E., Ban, N., Schär, C., and Somot, S.: Enhanced summer convective rainfall at Alpine high elevations in response to climate warming, Nature Geoscience, 9, 584–589, https://doi.org/10.1038/ngeo2761, 2016.

González-Hidalgo, J. C., Vicente-Serrano, S. M., Peña-Angulo, D., Salinas, C., Tomas-Burguera, M., and Beguería, S.: High-resolution spatio-temporal analyses of drought episodes in the western Mediterranean basin (Spanish mainland, Iberian Peninsula), Acta Geophysica, 66, 381–392, https://doi.org/10.1007/s11600-018-0138-x, 2018.

Greene, C. A., Thirumalai, K., Kearney, K. A., Delgado, J. M., Schwanghart, W., Wolfenbarger, N. S., Thyng, K. M., Gwyther, D. E., Gardner, A. S., and Blankenship, D. D.: The Climate Data Toolbox for MATLAB, Geochemistry, Geophysics, Geosystems, 20, 3774–3781, https://doi.org/10.1029/2019GC008392, 2019.

Grose, M. R., Syktus, J., Thatcher, M., Evans, J. P., Ji, F., Rafter, T., and Remenyi, T.: The role of topography on projected rainfall change in mid-latitude mountain regions, Climate Dynamics, 53, 3675–3690, https://doi.org/10.1007/s00382-019-04736-x, 2019.

Habib, M.: Evaluation of DEM interpolation techniques for characterizing terrain roughness, CATENA, 198, 105 072, https://doi.org/10.1016/j.catena.2020.105072, 2021.

Hanel, M., Rakovec, O., Markonis, Y., Máca, P., Samaniego, L., Kyselý, J., and Kumar, R.: Revisiting the recent European droughts from a long-term perspective, Scientific Reports, 8, 9499, https://doi.org/10.1038/s41598-018-27464-4, number: 1, 2018.

Hargreaves, G. H. and Samani, Z. A.: Reference Crop Evapotranspiration from Temperature, Applied Engineering in Agriculture, 1, 96–99, https://doi.org/10.13031/2013.26773, 1985.

Haslinger, K. and Blöschl, G.: Space-Time Patterns of Meteorological Drought Events in the European Greater Alpine Region Over the Past 210 Years: SPACE-TIME PATTERNS OF DROUGHT EVENTS, Water Resources Research, 53, 9807–9823, https://doi.org/10.1002/2017WR020797, number: 11, 2017.

Haslinger, K., Chimani, B., and Böhm, R.: 200 years of liquid and solid precipitation in major river systems originating in the Greater Alpine Region, pp. 1798–, 2012.

Hayes, M., Svoboda, M., Wilhite, D., and Vanyarkho, O.: Monitoring the 1996 Drought Using the Standardized Precipitation Index, Bulletin of The American Meteorological Society - BULL AMER METEOROL SOC, 80, 429–438, https://doi.org/10.1175/1520-0477(1999)080<0429:MTDUTS>2.0.CO;2, 1999.

Hoerling, M., Eischeid, J., Perlwitz, J., Quan, X., Zhang, T., and Pegion, P.: On the Increased Frequency of Mediterranean Drought, Journal of Climate, 25, 2146–2161, https://doi.org/10.1175/JCLI-D-11-00296.1, number: 6, 2012.

Hosking, J. R. M.: The theory of probability weighted moments, 1986.

Hosseini, T. S. M., Hosseini, S. A., Ghermezcheshmeh, B., and Sharafati, A.: Drought hazard depending on elevation and precipitation in Lorestan, Iran, Theoretical and Applied Climatology, 142, 1369–1377, https://doi.org/10.1007/s00704-020-03386-y, 2020.

IDMP: Drought and Water Scarcity, no. 1284 in WMO, Global Water Partnership, Stockholm, Sweden, 2022.

Karagulle, D., Frye, C., Sayre, R., Breyer, S., Aniello, P., Vaughan, R., and Wright, D.: Modeling global Hammond landform regions from 250-m elevation data, Transactions in GIS, 21, 1040–1060, https://doi.org/10.1111/tgis.12265, 2017.

Kulkarni, A. and Storch, H. v.: Monte Carlo experiments on the effect of serial correlation on the Mann-Kendall test of trend, volume: 4, 1995.

Kållberg, P. W., Simmons, A., Uppala, S., and Fuentes, M.: The ERA-40 archive. [Revised October 2007], 17, ECMWF, Shinfield Park, Reading, publication Title: ERA-40 Project Report Series, 2004.

Laimighofer, J. and Laaha, G.: How standard are standardized drought indices? Uncertainty components for the SPI & SPEI case, Journal of Hydrology, 613, 128 385, https://doi.org/10.1016/j.jhydrol.2022.128385, 2022.

McKee, T. B., Doesken, N. J., and Kleist, J. R.: THE RELATIONSHIP OF DROUGHT FREQUENCY AND DURATION TO TIME SCALES, 1993.

Mountain Research Initiative EDW Working Group: Elevation-dependent warming in mountain regions of the world, Nature Climate Change, 5, 424–430, https://doi.org/10.1038/nclimate2563, 2015.

Palazzi, E., Mortarini, L., Terzago, S., and Von Hardenberg, J.: Elevation-dependent warming in global climate model simulations at high spatial resolution, Climate Dynamics, 52, 2685–2702, https://doi.org/10.1007/s00382-018-4287-z, 2019.

Pavan, V., Antolini, G., Barbiero, R., Berni, N., Brunier, F., Cacciamani, C., Cagnati, A., Cazzuli, O., Cicogna, A., De Luigi, C., Di Carlo, E., Francioni, M., Maraldo, L., Marigo, G., Micheletti, S., Onorato, L., Panettieri, E., Pellegrini, U., Pelosini, R., Piccinini, D., Ratto, S., Ronchi, C., Rusca, L., Sofia, S., Stelluti, M., Tomozeiu, R., and Torrigiani Malaspina, T.: High resolution climate precipitation analysis for north-central Italy, 1961–2015, Climate Dynamics, 52, 3435–3453, https://doi.org/10.1007/s00382-018-4337-6, number: 5-6, 2019.

Pepin, N. C., Arnone, E., Gobiet, A., Haslinger, K., Kotlarski, S., Notarnicola, C., Palazzi, E., Seibert, P., Serafin, S., Schöner, W., Terzago, S., Thornton, J. M., Vuille, M., and Adler, C.: Climate Changes and Their Elevational Patterns in the Mountains of the World, Reviews of Geophysics, 60, https://doi.org/10.1029/2020RG000730, 2022.

Perosino, G. C. and Zaccara, P.: Elementi climatici del Piemonte, http://www.crestsnc.it/divulgazione/media/clima-piemonte.pdf, 2006.

Pörtner, H.-O., Roberts, D., Tignor, M., Poloczanska, E., Mintenbeck, K., Alegría, A., Craig, M., Langsdorf, S., Löschke, S., Möller, V., Okem, A., Rama, B., Belling, D., Dieck, W., Götze, S., Kersher, T., Mangele, P., Maus, B., Mühle, A., and Weyer, N.: Climate Change 2022: Impacts, Adaptation and Vulnerability Working Group II Contribution to the Sixth Assessment Report of the Intergovernmental Panel on Climate Change, https://doi.org/10.1017/9781009325844., 2022.

Rangwala, I. and Miller, J. R.: Climate change in mountains: a review of elevation-dependent warming and its possible causes, Climatic Change, 114, 527–547, https://doi.org/10.1007/s10584-012-0419-3, 2012.

Rasch, D., Kubinger, K. D., and Moder, K.: The two-sample t test: pre-testing its assumptions does not pay off, Statistical Papers, 52, 219–231, https://doi.org/10.1007/s00362-009-0224-x, 2011.

Robinson, N., Regetz, J., and Guralnick, R. P.: EarthEnv-DEM90: A nearly-global, void-free, multi-scale smoothed, 90m digital elevation model from fused ASTER and SRTM data, ISPRS Journal of Photogrammetry and Remote Sensing, 87, 57–67, https://doi.org/10.1016/j.isprsjprs.2013.11.002, 2014.

Sayre, R., Frye, C., Karagulle, D., Krauer, J., Breyer, S., Aniello, P., Wright, D. J., Payne, D., Adler, C., Warner, H., VanSistine, D. P., and Cress, J.: A New High-Resolution Map of World Mountains and an Online Tool for Visualizing and Comparing Characterizations of Global Mountain Distributions, Mountain Research and Development, 38, 240–249, https://doi.org/10.1659/MRD-JOURNAL-D-17-00107.1, 2018.

Shevlyakov, G. L. and Oja, H.: Robust correlation: theory and applications, Wiley series in probability and statistics, Wiley, Chichester, West Sussex, United Kingdom, 2016.

Terzago, S., Fratianni, S., and Cremonini, R.: Winter precipitation in Western Italian Alps (1926–2010): Trends and connections with the North Atlantic/Arctic Oscillation, Meteorology and Atmospheric Physics, 119, 125–136, https://doi.org/10.1007/s00703-012-0231-7, 2013.

Tigkas, D., Vangelis, H., and Tsakiris, G.: DrinC: a software for drought analysis based on drought indices, Earth Science Informatics, 8, 697–709, https://doi.org/10.1007/s12145-014-0178-y, number: 3, 2015.

Trenberth, K. E., Dai, A., Van Der Schrier, G., Jones, P. D., Barichivich, J., Briffa, K. R., and Sheffield, J.: Global warming and changes in drought, Nature Climate Change, 4, 17–22, https://doi.org/10.1038/nclimate2067, 2014.

Turco, M., Zollo, A. L., Ronchi, C., De Luigi, C., and Mercogliano, P.: Assessing gridded observations for daily precipitation extremes in the Alps with a focus on northwest Italy, Natural Hazards and Earth System Sciences, 13, 1457–1468, https://doi.org/10.5194/nhess-13-1457-2013, 2013.

Uboldi, F., Lussana, C., and Salvati, M.: Three-dimensional spatial interpolation of surface meteorological observations from high-resolution local networks, Meteorological Applications, 15, 331–345, https://doi.org/10.1002/met.76, 2008.

Unesco, ed.: Nature-based solutions for water, no. 2018 in The United Nations world water development report, UNESCO, Paris, 2018.

Vicente-Serrano, S. M., Beguería, S., and López-Moreno, J. I.: A Multiscalar Drought Index Sensitive to Global Warming: The Standardized Precipitation Evapotranspiration Index, Journal of Climate, 23, 1696–1718, https://doi.org/10.1175/2009JCLI2909.1, number: 7, 2010.

Vogel, J., Paton, E., Aich, V., and Bronstert, A.: Increasing compound warm spells and droughts in the Mediterranean Basin, Weather and Climate Extremes, 32, 100 312, https://doi.org/10.1016/j.wace.2021.100312, 2021.

Wada, Y., Flörke, M., Hanasaki, N., Eisner, S., Fischer, G., Tramberend, S., Satoh, Y., Van Vliet, M. T. H., Yillia, P., Ringler, C., Burek, P., and Wiberg, D.: Modeling global water use for the 21st century: the Water Futures and Solutions (WFaS) initiative and its approaches, Geoscientific Model Development, 9, 175–222, https://doi.org/10.5194/gmd-9-175-2016, 2016.

Wallemacq, P., Guha-Sapir, D., McClean, D., CRED, and UNISDR: The Human Cost of Natural Disasters - A global perspective, 2015.

Wang, W., Chen, Y., Becker, S., and Liu, B.: Variance Correction Prewhitening Method for Trend Detection in Autocorrelated Data, Journal of Hydrologic Engineering, 20, 04015 033, https://doi.org/10.1061/(ASCE)HE.1943-5584.0001234, 2015.

Ward, P. J., Blauhut, V., Bloemendaal, N., Daniell, J. E., De Ruiter, M. C., Duncan, M. J., Emberson, R., Jenkins, S. F., Kirschbaum, D., Kunz, M., Mohr, S., Muis, S., Riddell, G. A., Schäfer, A., Stanley, T., Veldkamp, T. I. E., and Winsemius, H. C.: Review article: Natural hazard risk assessments at the global scale, Natural Hazards and Earth System Sciences, 20, 1069–1096, https://doi.org/10.5194/nhess-20-1069-2020, 2020.

Welch, B. L.: The Generalization of 'Student's' Problem when Several Different Population Variances are Involved, Biometrika, 34, 28, https://doi.org/10.2307/2332510, 1947.

Whitehouse, D. J.: Handbook of surface metrology, Institute of Physics Publishing, Bristol, 1994.

World Meteorological Organization: Standardized precipitation index user guide., no. 1090 in WMO, Geneva, Switzerland, oCLC: 874098624, 2012.

Yevjevich, V. M.: Objective approach to definitions and investigations of continental hydrologic droughts, An, PhD Thesis, Colorado State University. Libraries, 1967.

Yue, S., Pilon, P., Phinney, B., and Cavadias, G.: The influence of autocorrelation on the ability to detect trend in hydrological series, Hydrological Processes, 16, 1807–1829, https://doi.org/10.1002/hyp.1095, 2002.